

FOURIER TRANSFORM INFRARED SPECTROSCOPIC TECHNIQUES  
FOR ANALYSIS OF ENGINEERING MATERIALS

by

NICHOLAS CONSTANTINE RIGAS

B.S., University of Missouri at Rolla, 1984

---

A THESIS

submitted in partial fulfillment of the  
requirements for the degree

MASTERS OF SCIENCE

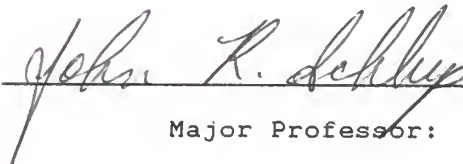
in

CHEMICAL ENGINEERING

Kansas State University  
Manhattan, Kansas

1988

Approved by:

  
Major Professor:

LD  
2668  
.T4  
CHE  
1988  
R54  
c. 2

ALL208 231753

## TABLE OF CONTENTS

### CHAPTER I

#### REVIEW OF FOURIER TRANSFORM INFRARED SPECTROSCOPY

Introduction .....	1
Review .....	I-1
Figure 1: Michelson Interferometer .....	I-7
References .....	I-8

### CHAPTER II

#### FTIR ANALYSIS OF FRACTURED COMPOSITES

Introduction .....	II-1
Review of Conventional FTIR Spectroscopic Techniques .....	II-2
Experimental .....	II-8
Discussion .....	II-11
Conclusion .....	II-14
Figure Captions .....	II-16
References .....	II-30

### CHAPTER III

#### PHOTOACOUSTIC SPECTROSCOPY

Microphone Detection .....	III-1
Photothermal Beam Deflection Detection .....	III-5
Figure Captions .....	III-10
References .....	III-15

### CHAPTER IV

#### CELL DESIGN

FTIR-PAS Cell Design .....	IV-1
FTIR-PBDS Cell Design .....	IV-4
Case Study: FTIR-PBDS Cell for Galvanic Corrosion Studies .....	IV-8
Figure Captions .....	IV-10
References .....	IV-14

### CHAPTER V

#### PHOTOACOUSTIC THEORY

Introduction .....	V-1
Theory .....	V-3
Discussion .....	V-14
Figure Captions .....	V-17
References .....	V-21

### CHAPTER VI

#### Initial Set-up of FTIR-PBD Spectrometer

General Set-up of FTIR-PBD Detection Scheme .....	VI-1
Initial Alignment Procedure for the PBD Experiment .....	VI-5
Discussion on the Kansas State University PBD Experiment .....	VI-8
Future Work .....	VI-12
Conclusions .....	VI-14
Figure Captions .....	VI-16
References .....	VI-23
Acknowledgements Abstract	

## INTRODUCTION

The scope of this thesis is to discuss the application of Fourier Transform Infrared Spectroscopy for in situ analysis of engineering materials. The material covered is not intended to be inclusive of all FTIR techniques available. An emphasis is placed upon the techniques which are applicable to in situ study of materials without requiring prior sample preparation, since the surface morphology can be altered. Of particular interest to the chemical engineer are reactions such as catalysis, electrochemical reactions, and environmental effects on materials.

The techniques available for use with FTIR spectroscopy are numerous. They include transmission, external reflection, attenuated total reflection, and diffuse reflection. To choose which technique can be properly used for analysis of materials, the capabilities and limitations of each must be known. A good case study to exam the capability of these spectroscopic techniques arose from the work by Jean Waters at Kansas State University on accelerated environmental testing of adhesive composites. It is known that water adsorption by the adhesive leads to a degradation in the mechanical properties of the material. It would be of particular interest to exam the fractured adhesive surface to determine changes in the molecular structure. This becomes a problem for most spectroscopic techniques since the fractured surface is very rough. The transmission, specular

reflection, attenuated total reflection, and a layer of KBr above the sample utilizing a diffuse reflection cell are examined for their application to analysis of the fractured surface.

The conventional transmission and reflection techniques mentioned above, the renewed interest in photoacoustic spectroscopy provides an alternative method for analyzing materials. Two types of detection schemes can be used with photoacoustic spectroscopy, microphone and photothermal beam deflection detection. The microphone detection suffers from the fact that the microphone is susceptible to damage by harsh reaction environments. On the otherhand the photothermal beam deflection detection scheme is not limited by the reaction environment. The advantages and disadvantages of each technique will be discussed.

To use photoacoustic spectroscopy for in situ analysis of surface reactions an understanding of cell design is needed. Cell design for the microphone detection scheme is discussed first since more work has been done for this type of sample cell. The requirements for designing a cell with microphone detection are similar to designing a cell for photothermal beam deflection detection. A case study is presented for the study of galvanic corrosion in metal matrix composites.

To better understand the photoacoustic effect in solids a simple one-dimensional mathematical model is developed.

This derivation specifically applies to the photothermal beam deflection detection scheme. The partial differential equations are put into dimensionless form. This form allows us to isolate the terms that influence the generation and intensity of the beam deflections. Trends can be observed for choice of modulation frequencies, deflection media, radiation intensity, and adsorptivity.

A Fourier transform infrared photothermal beam deflection experiment has been set-up. All components were specified to meet or exceed the requirements presented in the literature. The experiment has been brought up to the point where as steady-state deflection is observed in the laser beam when the infrared source is on. As of yet no centerburst has been found. Future work will focus on reducing the noise levels to locate the centerburst.

## CHAPTER I

### REVIEW OF FOURIER TRANSFORM INFRARED SPECTROSCOPY

Fourier transform infrared (FT-IR) spectroscopy is an analytical tool useful not only to the chemist, but also to the chemical engineer modeling a chemical process with data generated by it. This analytical technique has numerous sampling methods in its arsenal, extending its capability into solid, liquid, and gas phase samples. To properly utilize FT-IR spectroscopy for a specific need, a chemical engineer must know the capabilities and limitations of each sampling method. Current developments in FT-IR photoacoustic spectroscopy, including microphone and photothermal beam deflection detection schemes, provide a new appeal for applications of FT-IR to engineering problems by providing data in situ. Of particular interest are solid/gas and solid/liquid surface reactions including catalysis, electrochemical reactions, and corrosion.

The application of infrared spectroscopy as an analytical tool for the investigation of "disturbed molecules" was first developed by W.M. Coblentz in the 1880's. He determined that the spectra obtained were related to the vibrational and rotational energy states of the molecules. Infrared spectroscopy branched off into two methods, dispersive and interferometric spectroscopy. The dispersive method utilizes a grating or prism to disperse the radiation into its individual spectral elements measuring the energy

for each spectral band in the frequency domain. The vibrational and rotational absorption bands are observed directly from the spectra [1].

In the interferometric method the infrared radiation is split into two optical paths then recombined after a path difference is introduced [1]. These recombined beams interfere constructively if the beams are in phase, and destructively when out of phase. The path difference is referred to as the optical retardation. The intensity of the radiation reaching the detector is a function of retardation, and consists of a dc component and an ac component. The modulated, ac, component is the interferogram. The centerburst is defined as the portion of the interferogram when the optical retardation is equal to zero.

Both Michelson and Lord Rayleigh realized that it would be possible to obtain the infrared spectrum of a sample by taking the Fourier transform of an interferogram. The dual-beam Fourier Transform Infrared spectrometer was developed by Michelson's in the 1880's. A schematic of the simplest form of the Michelson interferometer is shown in Figure 1. Michelson's interferometer consists of a radiation source, beamsplitter, fixed mirror, and a movable mirror. The beamsplitter is positioned at a 45 degree angle to the radiation source. In the ideal case it allows 50% of the light to pass and deflects 50% of the light 90 degrees. Note that a 50/50 beam splitter exists only in theory; in



reality some of the light is absorbed by the beam-splitter. The fixed and moving mirror are positioned perpendicular to one another allowing them to each accept 50% of the split radiation. The composition of the beam splitter depends upon the region of the spectra being monitored. This is required since the ideal beam splitter would not absorb any of the radiation in the region of the infrared spectrum being investigated. In the mid-infrared (MIR) region of the spectrum a germanium coated potassium bromide (KBr) beamsplitter is used. The KBr beam splitter absorbs above 4000  $\text{cm}^{-1}$  and below 400  $\text{cm}^{-1}$ , making it ideal for the MIR region 3800  $\text{cm}^{-1}$  to 600  $\text{cm}^{-1}$ .

Phase differences in the radiation are introduced by the moving mirror. The optical path difference, or retardation, is twice the difference between the distance of the moving mirror from the beamsplitter and the distance of the fixed mirror from the beamsplitter. This retardation causes phase differences to occur upon recombination of the beams at the beamsplitter. These phase difference cause constructive and destructive interference upon recombination at the beam splitter, resulting in the observed interferogram. For a constant velocity moving mirror the intensity of the radiation at the detector is given by the following equation [2].

$$I'(\delta) = 0.5 I(\delta) \{ 1 + \cos(2\pi v \delta) \} \quad (1)$$

where



$I'(\delta)$  = The intensity of the radiation at  
the detector as a function of  
optical retardation [Watts/cm<sup>-1</sup>]

$\delta$  = Optical retardation [cm]

$\nu$  = Wavenumber [cm<sup>-1</sup>]

As stated earlier the intensity consists of a dc component,  $0.5I(\delta)$ , and an ac component,  $0.5I(\delta)\cos(2\pi\nu\delta)$ . The inteferogram is the modulated component, which is dependant upon optical retardation, wavenumber, and the intensity of the infrared source.

The Michelson interferometer didn't come under study again until 50 years after its invention, when interest in the far infrared (FIR) region of the spectrum began. FIR, from 700 cm<sup>-1</sup> to 150 cm<sup>-1</sup>, is the low energy region of the electromagnetic spectrum. The dispersive instrument, already hampered by the loss of energy due to the slits, allows little or no energy to reach the detector when monitoring the FIR region. Interferometers had the advantage over the dispersive instruments of allowing more energy to reach the detector since no slits are used.

The lack of computers to do the Fourier transform of the interferogram initially made FTIR spectroscopy impractical to be used anywhere but in the FIR region of the spectrum. Too many calculations were required by hand to Fourier transform the interferogram into the frequency spectrum in the NIR and MIR regions. The number of hand calculations required for the FIR were considerably less. With

the coming of the computer age, FTIR spectroscopy was quickly expanded into the MIR and NIR regions of the spectrum.

The most important advantage of FTIR interferometers over dispersive instruments is known as Fellgett's advantage. Multiplexing, as it is known, is used to enhance the signal to noise ratio (SNR) and to acquire data much faster than with a dispersive instrument [1]. The SNR is directly proportional to the square root of the time required to measure one scan of the spectral range [2]. Since all frequencies of interest are sampled simultaneously in FT-IR spectroscopy the interferogram can be obtained in  $1/N$  the time of a dispersive unit, where  $N$  is the number of spectral frequencies. Increasing the number of scans,  $n$ , increases the SNR by the square root of  $n$ . This is due to the fact that the noise in the IR detectors is random. By signal averaging the noise level is reduced while the signal level is increased [2].

FTIR spectroscopy has the inherent advantage of allowing more radiation to reach the detector than a dispersive instrument. This becomes crucial for the FIR region while is less important in the higher energy near infrared (NIR) and ultraviolet (UV) regions. The amount of energy allowed to reach the detector in a FTIR instrument is referred to as Jacquinot's advantage. The ratio of the throughput of a FTIR instrument versus a dispersive instrument is propor-

tional to the wavenumber squared. At higher wavenumbers Jacquinot's advantage can be quite high and becomes less important at the lower wavenumbers [2].

The high precision measurement of the spectral frequencies using lasers contained within the instrument is known as Connes advantage [1]. Specifically He-Ne lasers are being installed in the newer instruments. Incorporating a He-Ne laser allows for the optical retardation to be digitized in equal well-defined intervals. An unaligned laser will cause a wavenumber shift in the spectra. Since the shift is a linear function of wavenumber, the shift can be corrected by adjusting the laser wavenumber parameter in the transform program.

FTIR spectroscopy has emerged as one of the most versatile and cost effective analytical tools available to the scientist. Numerous sample cells have been developed to allow for analysis of gases, liquids, and condensed phase samples. The cells available for condensed phase analysis will be discussed. Some of these techniques apply to gas and liquid spectroscopic analysis as well.

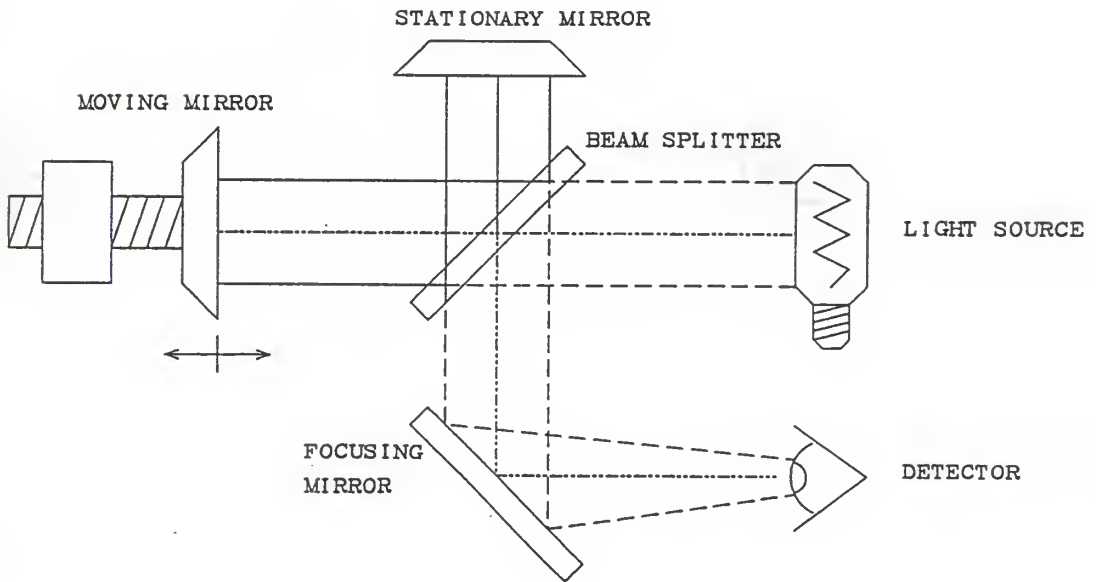


Figure 1: A schematic diagram of a simple Michelson interferometer.

References

- (1) Grim, W.M. III and W.G. Fatel, Fourier Transform Infrared Spectroscopy, T. Theophanides (Eds.), pp.25-42, D. Reidel Publishing Co. (1984).
- (2) Griffiths P.R. and J.D. Haseth, Fourier Transform Infrared Spectroscopy, pp.1-6, Wiley, New York (1986).

## CHAPTER II

### FOURIER TRANSFORM INFRARED ANALYSIS OF FRACTURED COMPOSITE SURFACE

#### INTRODUCTION

Analysis of fractured adhesive surfaces would be important to the composite industry. Exposure of adhesively bonded composite samples to high temperature and humidity leads to degradation of the mechanical properties. Lap shear strength data obtained from composite samples show that water absorption has a detrimental effect on the mechanical shear strength of the material [1,2]. FTIR analysis of fractured adhesive surfaces would provide information on the chemical changes that have occurred as a consequence of water absorption. The molecular characterization of fractured adhesive surfaces utilizing FTIR spectroscopy could then be used to provide an explanation for the changes in mechanical properties.

The surface of a fractured adhesive composite is quite rough. This can pose a problem when using conventional FT-IR spectroscopic techniques such as attenuated total reflectance and specular reflection which require a smooth surface. Other techniques like transmission require sample preparation which alter the sample's surface morphology. To analyze the fractured surface using FT-IR spectroscopy, a sampling technique must be used that requires a minimal amount of sample preparation. Sample preparation can affect

the samples morphology and introduce erroneous information in to the spectra [3]. The ideal technique would allow for spectra to be obtained in situ. Chemical changes would be observed in the adhesive as water was absorbed.

Conventional FT-IR spectroscopic techniques including transmission, specular reflection, and attenuated total reflectance have been examined for their applicability for analysis of fractured adhesive surfaces. A technique, developed by Koenig etal., in which the diffuse reflection infrared Fourier transform (DRIFT) cell is utilized along with a layer of KBr powder over the sample surface, is examined for spectroscopic analysis of fractured adhesive surfaces. Spectra obtained by this method are then compared against the conventional techniques.

#### REVIEW OF CONVENTIONAL FTIR SPECTROSCOPIC TECHNIQUES

Transmission spectroscopy monitors the amount of infrared energy that is transmitted through a sample. The sample is usually positioned at the focus of the infrared beam so as to maximize the energy density at the sample (Figure 1). The conventional transmission method used in FT-IR spectroscopy is not suitable for analysis of fractured adhesive surfaces. To use this sampling technique, a layer of the polymer adhesive would have to be removed from the fractured surface. This would be impossible to accomplish with a cured composite sample.



The intensity of infrared radiation transmitted is represented by the following equation when reflections are ignored [5].

$$I = I_0 \times 10^{-abc} \quad (1)$$

where

$I_0$  = Incident beam of radiation.

$a$  = absorptivity

$b$  = sample thickness

$c$  = sample concentration

The absorption of infrared radiation,  $a$ , and the sample thickness,  $b$ , for most polymer samples is quite high. In addition, the adhesive concentration,  $c$ , and surface morphology cannot be controlled with a fractured surface of adhesively bonded composites. Equation 1 shows that in the case of polymer samples little to no radiation is transmitted. Sample preparation can reduce the thickness of the adhesive layer and its concentration, but this will change the sample morphology. However, transmission FT-IR spectroscopy is useful for providing reference spectra on the uncured adhesives and on cast films of cured adhesives.

The surface irregularities of a fractured adhesive composite can pose a problem to the specular reflection technique. Irregularities lead to scattering of the specular component of reflection causing less energy to reach the detector. Scattering can be reduced by increasing the angle of incidence of the IR beam. The band intensities in specu-

lar reflection spectra depend upon the angle of incidence of the infrared radiation at the sample surface.

For IR radiation with its electric vector polarized perpendicular (p-polarization) to the surface, large angles of incidence provide the optimum sensitivity. A loss of spectral sensitivity would be expected with no p-polarization of the infrared beam. Dispersion of the index of refraction impacts the specular reflection spectra. High adsorption at a given wavelength can lead to anomalies in the line shape. This dispersion spectra appears as a result of the complex index of refraction (Figure 2). By increasing the angle of incidence and polarizing the incident radiation these bands can be eliminated for a smooth surface sample. A rough surface sample, like the fractured adhesive, scattering cannot be controlled and the dispersion effects may not be eliminated.

Attenuated Total Reflectance (ATR) is a non-destructive technique requiring little to no sample preparation. The sample is brought into intimate contact with an optical element where it interacts with the evanescent wave (Figure 3). The depth of penetration of the infrared radiation into the sample is governed by the following equation.

$$d = \lambda_0 / \{2\pi n_s (\sin\theta - n_{sc})\} \quad (2)$$

where

$d$  = the depth of penetration of the infrared beam into the sample

$\lambda_0$  = the wavelength of interest

$\theta$  = angle of incidence of the radiation source with the sample surface.

$n_c$  = the refractive index of the crystal

$n_s$  = the refractive index of the sample

$n_{sc} = n_s / n_c$

By varying the angle of incidence, the depth of IR penetration into the sample can be controlled.

ATR spectroscopy requires good sample-to-crystal contact. If intimate contact is lacking, optical cavities are introduced leading to higher and lower contrast spectra. The effects from these optical cavities cause a different wavelength dependance for the depth of penetration. The fractured adhesive samples provide a rough surface which prevents intimate contact between the crystal and the sample. The hardness of a cured adhesive restricts the amount of pressure that can be applied to the crystal to increase contact without risk of damaging the crystal. The added pressure distorts significantly the surface morphology of the fractured sample.

Attenuated total reflectance cannot be used on fractured composite surfaces because the surface irregularities of the sample which prohibit intimate contact with the crystal. This technique would be useful for FT-IR spectros-

copic analysis of cast film sample of the adhesive that haven't undergone mechanical testing. In situ analysis would be limited because the intimate contact between the sample surface and crystal inhibits water adsorption at the surface being observed.

A sampling technique that has been used largely for powdered samples is diffuse reflection infrared Fourier transform (DRIFT) spectroscopy (Figure 4). DRIFT is known for its high sensitivity. This method has been shown to be applicable for analysis of chemical species adsorbed onto powders. DRIFT spectroscopy is sensitive to particle size, sample concentration, and optical geometry effects. The specular reflection component introduces reststrahlen bands into the DRIFT spectra. Recent developments in cell design have allowed for the elimination of the specular component and monitoring of the diffuse component of powders. Decreasing the concentration of sample, a deeper penetration of the infrared radiation is established reducing the unwanted surface scattering effects. DRIFT does not lend itself as a useful technique for FTIR analysis of fractured adhesive samples. Obtaining data with a DRIFT cell on a polymer surface would produce essentially a specular reflection spectrum.

A technique has been developed incorporating the basic DRIFT cell for the study of condensed phase polymer samples by introducing a layer of KBr powder over the sample to

obtain realizable spectra [4]. The KBr overlayer provides a medium in which isotropic scattering of the IR radiation occurs prior to contact with the sample surface. Scattering of the radiation increases the surface reflection and decreases the absorption into the sample, making this a more surface sensitive technique. The KBr overlayer provides a means of eliminating the specular component and enhancing the diffuse component of reflection. Reducing the specular component of reflection eliminates the reststrahlen bands in the spectra caused by the dispersion effects. This technique provides a means of analyzing fractured adhesive surfaces. No sample preparation is required and it is a non-destructive technique.

The KBR overlayer method is sensitive to the volume of KBr used and its particle size distribution. The amount of infrared scattering in the KBr overlayer above the sample is important for reducing the specular reflection component and depth of penetration into the bulk polymer. As the layer of KBr over the sample increases, the amount of scattering is enhanced, and therefore, fewer rays reach the sample reducing the amount of infrared radiation penetrating into the bulk of the sample. Consequently, by increasing the amount of KBr over the sample surface one ensures that the surface will be analyzed rather than the bulk material [6]. Increasing the amount of KBr overlayer beyond the optimum depth used for analysis leads to a decrease in spectral sensitivity and reduces peak intensities. A decrease in the

particle size of the KBr powder increases its dispersion coefficient [6]. Spectra of polymer fibers has been obtained utilizing this overlayer technique [6]. A larger dispersion coefficient insures a more thorough isotropic scattering of the radiation.

## EXPERIMENTAL

Two paste adhesive samples both diglycidyl ethers with bisphenol A (DGEBA), EA9304.1 developed by 3M Corp., and EC3448 developed by the Hysol Inc., were provided by Beech Aircraft. The cast film adhesive samples were used for investigating the KBr overlayer method and for comparing this technique with transmission, specular reflection, and attenuated total reflectance. These cast films were cured at Beech Aircraft per company specification. One set of adhesive samples had undergone 80% prebond humidity exposure while the other set was exposed to room humidity only. The adhesively bonded composite samples were layed-up and cured at Beech per company specifications. The cast film and composite samples were both fabricated from EA9304.1 and EC3448 paste adhesive. Adhesively bonded epoxy-carbon fiber composites underwent accelerated enviromental testing in humidity chambers at Kansas State University. Mechanical strengths were then obtained via lap shear tests. After being tested, the fractured samples were sealed in plastic bags and kept in dessicators to await FTIR analysis.

A Nova Cygni 120 spectrophotometer manufactured by Mattson Instruments, Inc. with a germanium coated KBr beam-splitter was used to obtain all the spectra. A liquid nitrogen cooled MCT detector was utilized for the techniques, except for the transmission experiment in which a TGS detector was used. The data were acquired at 4 wavenumber resolution between 400 and 4000  $\text{cm}^{-1}$ . The transmission accessory, the specular reflection, and attenuated total reflection cells were purchased from Mattson Instruments. A Harrick Scientific DRA-2CO DRIFT cell was utilized for the overlayer technique.

A special sampling cup was designed at Kansas State University for the KBr overlayer DRIFT technique. This cup fits directly into the DRA-2CO DRIFT cell replacing the standard sampling cup. The design of the cup (Figure 5) allowed for the depth of KBr to be varied while keeping the height of the cup at the optimum value. The sampling cup was fabricated from stainless steel.

Spectrophotometric grade KBr was dried in a nitrogen environment at 80 C over night. The KBr powder was ground with an agate mortar and pestle just prior to use in the overlayer technique. For this initial application of the overlayer method no sieves were used to control the particle size of the KBr powder.

For investigating the KBr overlayer method, the cast films of the adhesives were cut with a pair scissors in a



circular pattern to cover the bottom of the special sampling cup. Plugs were punched with a hole puncher from the fractured adhesive composite again to cover the bottom of the sampling cup. The height of the sampling cup was adjusted, based upon the top of the sampling cup to the base of the DRIFT cell, to maximize the energy throughput to the detector. The KBr overlayer thickness varied from 0.0 inches to 0.10 inches in .005 inch increments to determine the optimum depth. A 30 minute purge with air dried and scrubbed of CO was done prior to data acquisition so as to minimize the water and CO absorption. 256 scans were coadded per experimental run enhance the signal-to-noise ratio.

Shavings of the cast film samples were taken and ground with dried KBr to prepare the sample for the transmission experiment. A pellet was pressed and transmission spectra obtained. For the specular reflection method and attenuated total reflection methods samples were cut from the cast film adhesive to the appropriate shape and size. A sample was placed on each side of the KRs-5 crystal for the ATR technique.

All spectra were reported in absorbance units except for the overlayer technique. The KBr overlayer technique spectra were recorded using the Kubelka-Munk function. Software developed by Mattson Instruments were used for integration of the O-H bands in the spectra. Using the software a reference peak was chosen such that its intensity

did not vary between spectra. Then two frequencies were specified above and below the peak to be integrated. The ratio representing the area under the peak of interest over the area under the reference peak was generated.

## DISCUSSION

The changes in chemical structure of the EA9304.1 adhesive can be clearly seen in Figures 6 and 7. The top spectra in Figures 6 and 7 represents this DGEBA epoxy paste adhesive exposed to room humidity prior to curing while the lower spectra is that of the same material exposed to 80% humidity prior to curing. These spectra were obtained using the transmission technique. The C=N peak at 2172  $\text{cm}^{-1}$  is present in the low humidity spectra while it disappears under high humidity conditions. The presence of the C=N's stretches in the low humidity sample maybe indicative of a incompletely cured sample. C=N sites are susceptible to reaction with adsorbed water. To fully examine this hypothesis adhesive samples prior to cure would have to be examined also. The ester C=O stretch at 1736  $\text{cm}^{-1}$  and C-O band at 1235  $\text{cm}^{-1}$  diminish in intensity in the high humidity sample, further indicating chemical changes upon water adsorption (Figure 7). The growth of the carboxylate band at 1651  $\text{cm}^{-1}$  with water adsorption supports that pre-bond water absorption by the adhesive is altering its chemical structure. Integration of the O-H band above 3000  $\text{cm}^{-1}$  reveals a increase by a factor of 1.5 in O-H concentration in the high

humidity sample. A similar analysis for EC3448 shows a two-fold increase in O-H concentration in the high humidity as compared to room humidity exposure. No noticeable changes in chemical structure of EC3448 are observed (Figure 8).

The 25 mil KBr layer over the sample provides the best spectral resolution (Figure 9). The O-H stretch above 3000  $\text{cm}^{-1}$ , C-H stretch just below 3000  $\text{cm}^{-1}$ , and the aromatic overtones at 2068  $\text{cm}^{-1}$  and 1883  $\text{cm}^{-1}$  are clearly visible. The fingerprint region below 2000  $\text{cm}^{-1}$  becomes distorted due to band broadening, although the general shape of region is defined. Increasing the depth of KBr over the sample surface leads to a decrease in the spectral sensitivity of the spectra (Figure 9). This agrees with the theory that as the KBr overlayer is increased, the scattering of the infrared radiation is too great for any of the radiation to return to the sampling optics of the DRIFT cell. Eventually at depths over 80 mils, no IR radiation leaves the KBr overlayer and reaches the detector.

The KBr overlayer provides the needed scattering of the IR radiation prior to impinging the sample surface, eliminating the dispersion effects in the spectra (Figure 10). The spectra representing zero KBr overlayer and specular reflection data are quite similar. The similarities can clearly be seen in the fingerprint region below 2000  $\text{cm}^{-1}$ . This supports the notion that utilizing the DRIFT accessory

for analysis of a solid without a KBr overlayer leads to specular reflection spectra.

A comparison of the transmission, attenuated total reflection, specular reflection, and KBr overlayer spectra of the cast film adhesive samples are shown in Figure 11. The distortion of the ATR spectra above 3000  $\text{cm}^{-1}$  and the dispersion effects in the specular reflection data might be eliminated by increasing the angles of incidence. Better data using the specular reflection cell might be obtained by going to grazing angles of incidence. The 25 mil overlayer gives spectra similar to the transmission data above 2000  $\text{cm}^{-1}$ .

Data have been obtained on fractured adhesive surfaces with the KBr overlayer technique. The irregularities in the topography of the fractured surface were much more severe than those of the cast film samples. The optimal depth of KBr was increased from 25 mils to 45 mils to compensate for the increased surface roughness of the fractured surfaces and provide a thick enough layer for isotropic scattering of the infrared radiation. Spectra of adhesively bonded samples, A19 and A72, both having undergone high humidity pre-bond exposure are shown in Figure 12. Accompanying each fractured surface spectra is a reference spectra of the high humidity cast film samples EA9304.1 and EC3448, respectively. A reference peak at 1883  $\text{cm}^{-1}$  was chosen for integration of the O-H stretch in the high humidity frac-

tured sample A19 versus the low humidity fractured sample A60. This aromatic overtone peak was chosen since its intensity is not expected to change upon exposure of the adhesive to high pre-bond moisture. The integration of the areas under the O-H stretches reveal a increase in O-H concentration by a factor of 1.5 in the high humidity sample A19.

## CONCLUSION

Chemical changes in the adhesives EA9304.1 and EC3448 upon adsorption of water can be detected using FT-IR spectroscopy. The spectra provide a means of quantifying such chemical changes due to water adsorption. Transmission, attenuated total reflectance, and specular reflection are not well suited for analysis of fractured adhesive surfaces. The KBr overlayer technique was verified as a viable alternative technique for analysis of fractured adhesive surfaces.

The depth of KBr over the sample surface will depend on the sample's surface topography. A rougher surface requires more KBr to achieve isotropic scattering of infrared radiation. The KBr overlayer technique as it stands does not allow for the fingerprint region of the spectra below 2000  $\text{cm}^{-1}$  to be visible, although the O-H, C-H, N-H, and aromatic overtone stretches are clearly resolved above 2000  $\text{cm}^{-1}$ . This suggests that the particle size distribution of the KBr

should be decreased and controlled to isotropically scatter the larger wavelengths. If the particle size distribution is decreased, the needed amount covering the sample surface would decrease, although the amount of KBr required would still depend upon the roughness of the fractured surface.

The quantitative data obtained for the increase in O-H concentration upon high humidity exposure assume that the amount of water absorbed by the adhesive is homogeneous. This assumption is needed since the exact location at which the adhesive will fracture cannot be predetermined. For these samples, the assumption would hold since they were kept under humidity exposure until no more weight gain due to water absorption was observed, indicating that a state of equilibrium was reached.

Future work must focus on controlling the particle size distribution of the KBr in order to better resolve the fingerprint region of the spectra. Sample spectra of the adhesives prior to cure are needed as a references. Photoacoustic spectroscopy should be examined as another alternative for fractured surface analysis. Eventually techniques like photoacoustic spectroscopy will be investigated to monitor the chemical changes of the adhesives in situ as water is adsorbed.



FIGURE CAPTIONS

1. A schematic diagram of the transmission technique.
2. A schematic diagram of the specular reflection technique. The equations for reflectivity as a function of the indices of refraction is given. The dispersion effects in reflectivity due to the differences in index of refraction is schematically outlined for the three cases.
3. A schematic diagram of the attenuated total reflectance technique.
4. A schematic diagram of the diffuse reflection infrared Fourier transform cell incorporating ellipsoidal mirrors.
5. The KBr overlayer sampling cup. The platform on which the sample sits is threaded so as to allow for adjustment to control the depth of KBr. The sampling cup height off the DRIFT cell base is adjusted to maximize the energy throughput.
6. FT-IR transmission spectra of EA9304.1 cast film adhesive samples from 4000  $\text{cm}^{-1}$  to 400  $\text{cm}^{-1}$ . (a) Room humidity prebond exposure. (b) 80% humidity prebond exposure.
7. Enlargement of the fingerprint region from 2250  $\text{cm}^{-1}$  to 500  $\text{cm}^{-1}$  of Figure 6.
8. FT-IR transmission spectra of EC3448 cast film adhesive sample from 4000  $\text{cm}^{-1}$  to 400  $\text{cm}^{-1}$ . (a) Room humidity prebond exposure. (b) 80% humidity prebond exposure.
9. FT-IR spectra of EC3448 80% humidity prebond exposure using various depths of KBr overlayer. (a) Transmission spectra as a reference. (b) 25 mil KBr overlayer. (c) 45 mil KBr overlayer. (d) 65 mil KBr overlayer.
10. 0 mils KBr overlayer and specular reflection spectra of EC3448 80% humidity prebond exposure cast film sample. (a) Transmission spectra as a reference. (b) 25 mil KBr overlayer as a reference. (c) 0 mil KBr overlayer. (d) Specular reflection spectra.
11. FT-IR spectra of EC3448 80% humidity prebond exposure. (a) Transmission. (b) Attenuated Total Reflectance. (c) Specular reflection. (d) 25 mil KBr overlayer.



12. 45 mil KBr overlayer spectra of fractured adhesive samples. (a) A19 80% humidity prebond exposure. (b) EA9404.1 80% humidity prebond exposure cast film adhesive. (c) A72 room humidity prebond exposure. (d) EA9304.1 room humidity prebond exposure cast film adhesive.

# TRANSMISSION

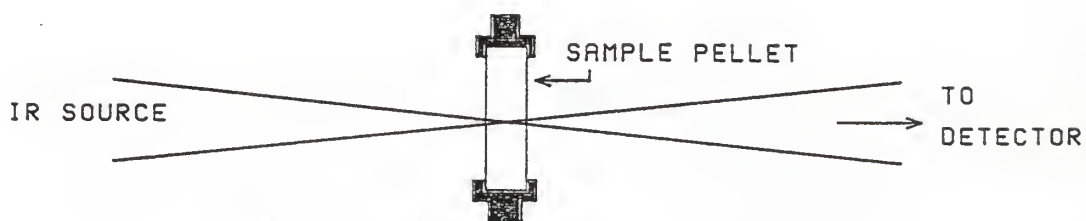
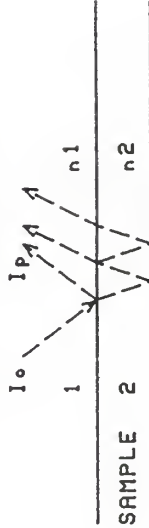


Figure 1: A schematic diagram of the transmission technique.

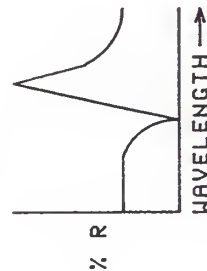
# SPECULAR REFLECTION



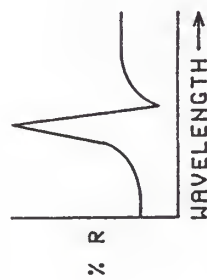
$$R = \text{REFLECTIVITY} = \frac{(n_2 - n_1)^2}{(n_2 + n_1)^2}$$

## 3 CASES:

1)  $n_1 < n_2$



2)  $n_2 < n_1$



3)  $n_2 = n_1$

- NO REFLECTION OCCURS UNTIL THE VALUES OF  $n_2$  AND  $n_1$  DEVIATE. WHEN A MISMATCH IN THE ABSORPTION BANDS OCCUR, TWO SHARP BANDS APPEAR ON EITHER SIDES OF THE MAXIMUM ABSORPTION.

Horriek, N.J., " Internal Reflection Spectroscopy " Harriek Corp., 1979.

Figure 2: A schematic diagram of the specular reflection technique. The equations for reflectivity as a function of the indices of refraction is given. The dispersion effects in reflectivity due to the differences in index of refraction is schematically outlined for the three cases.

# ATTENUATED TOTAL REFLECTANCE (ATR)

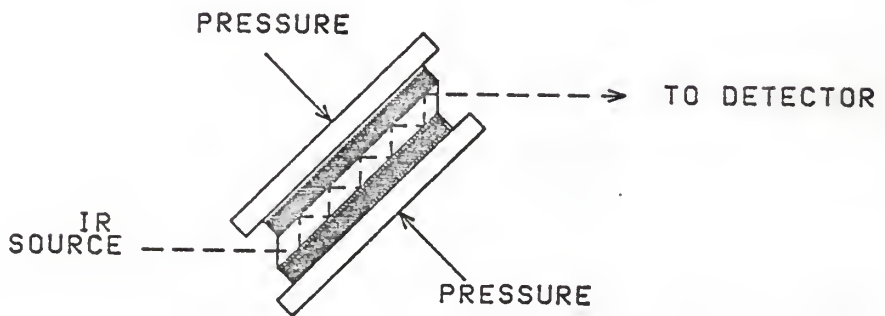


Figure 3:A schematic diagram of the attenuated total reflectance technique.

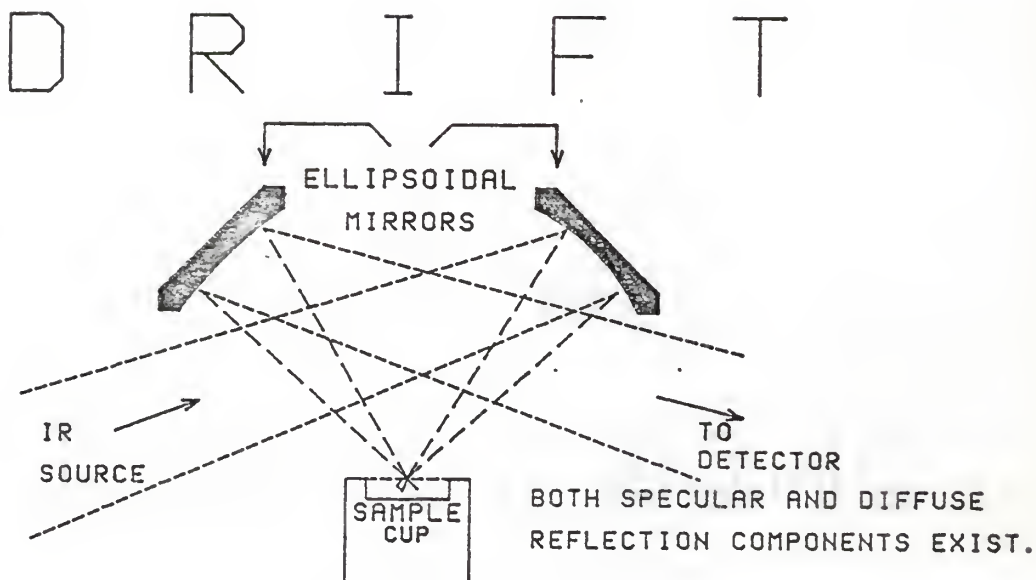


Figure 4: A schematic diagram of the diffuse reflection infrared Fourier transform cell incorporating ellipsoidal mirrors.

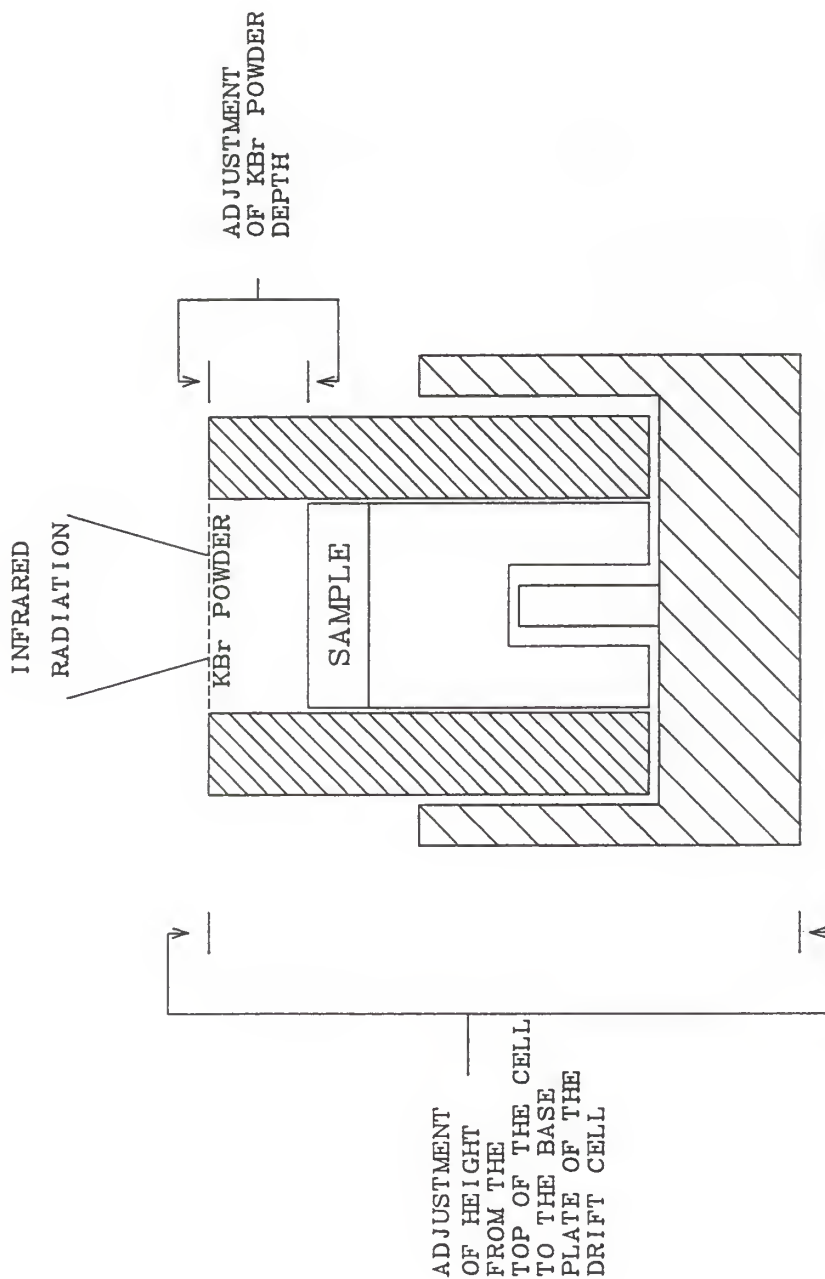


Figure 5: The KBr overlayer sampling cup. The platform on which the sample sits is threaded so as to allow for adjustment to control the depth of KBr. The sampling cup height off the DRIFT cell base is adjusted to maximize the energy throughput.

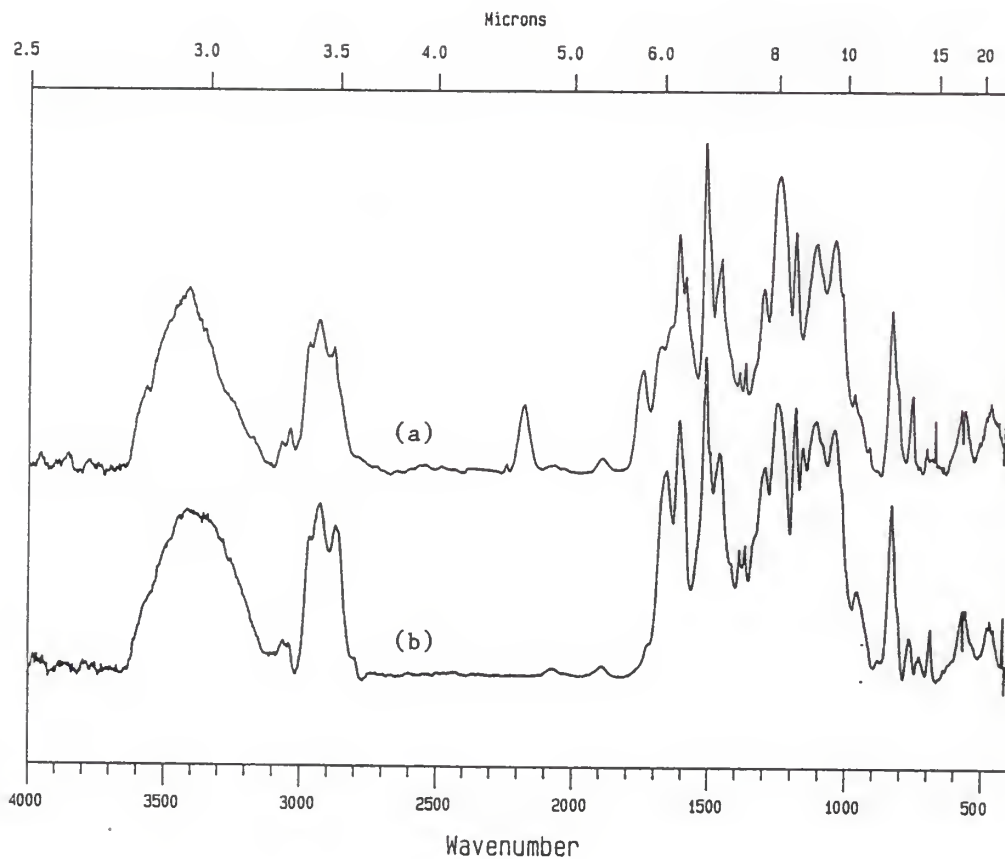


Figure 6: FT-IR transmission spectra of EA9304.1 cast film adhesive samples from 4000 cm<sup>-1</sup> to 400 cm<sup>-1</sup>. (a) Room humidity prebond exposure. (b) 80% humidity prebond exposure.



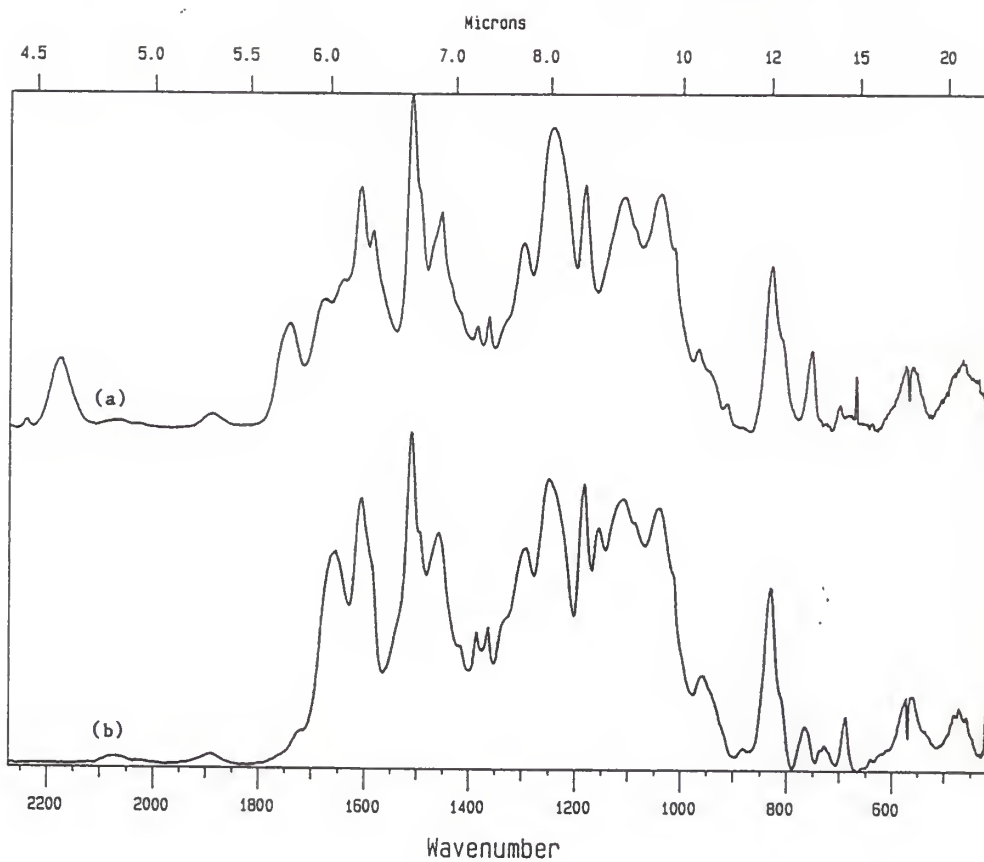


Figure 7: Enlargement of the Fingerprint region from 2250 cm<sup>-1</sup> to 500 cm<sup>-1</sup> of Figure 6.

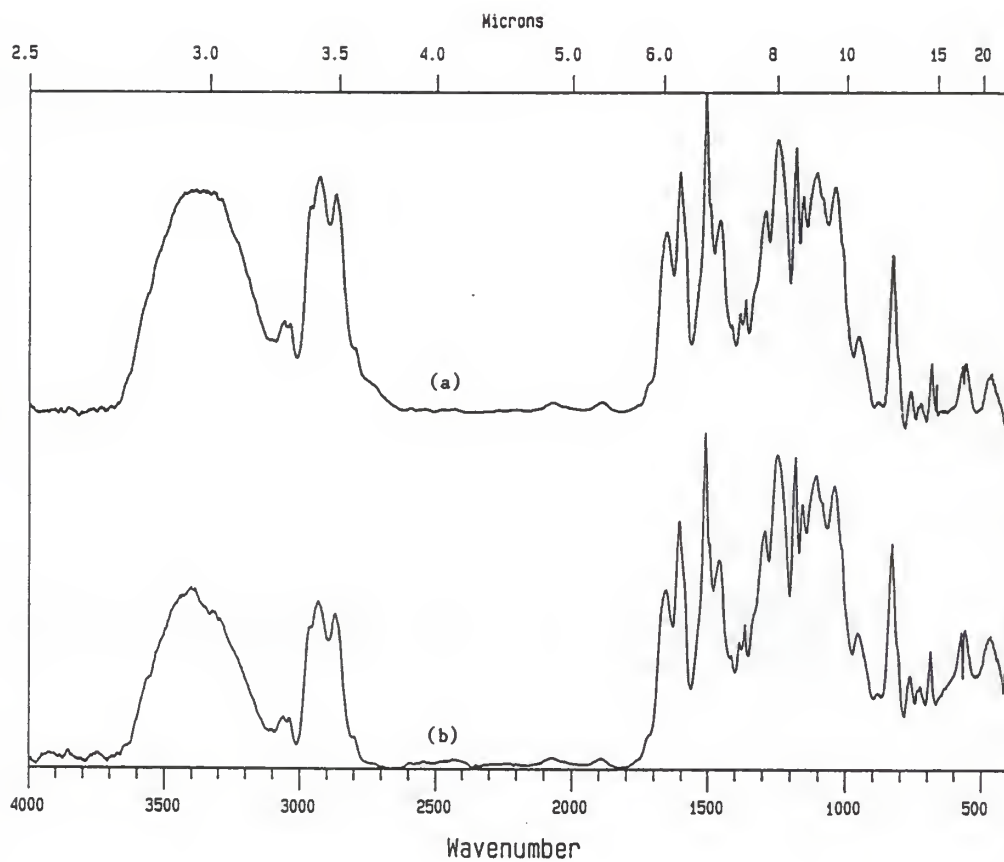


Figure 8: FT-IR transmission spectra of EC3448 cast film adhesive sample from 4000 cm<sup>-1</sup> to 400 cm<sup>-1</sup>. (a) Room humidity prebond exposure. (b) 80% humidity prebond exposure

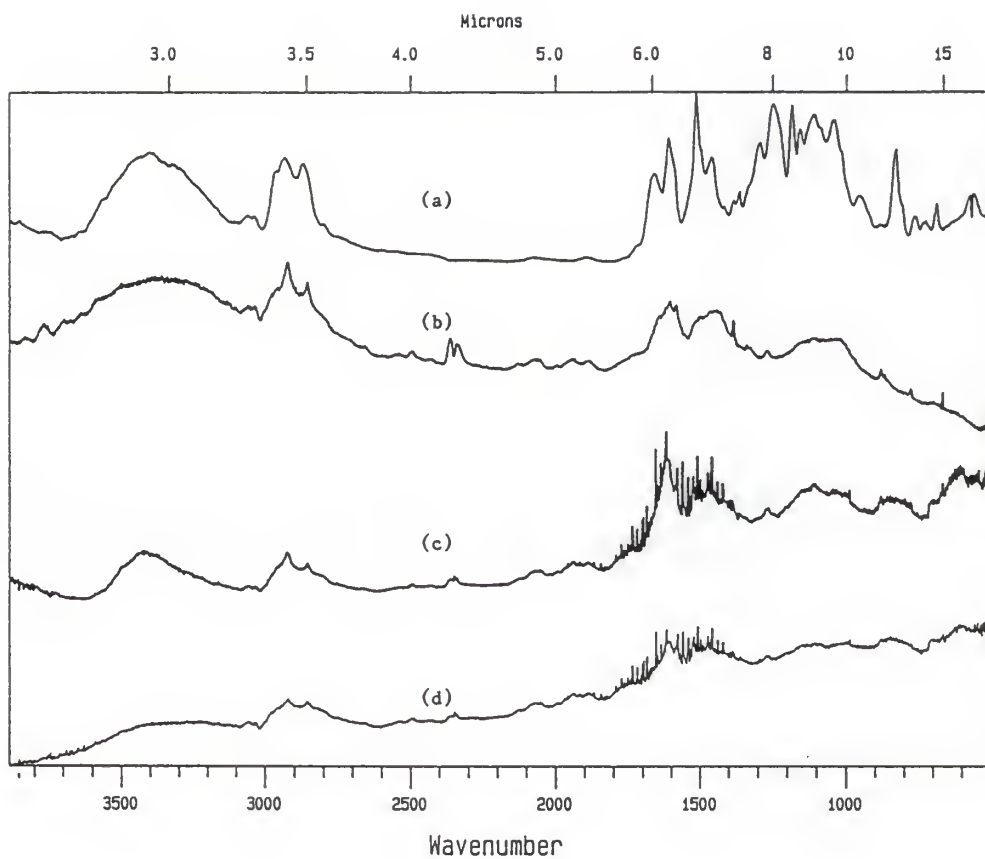


Figure 9: FT-IR spectra of EC3448 80% humidity prebond exposure using various depths of KBr overlayer. (a) Transmission spectra as a reference. (b) 25 mil KBr overlayer. (c) 45 mil KBr overlayer. (d) 65 mil KBr overlayer.

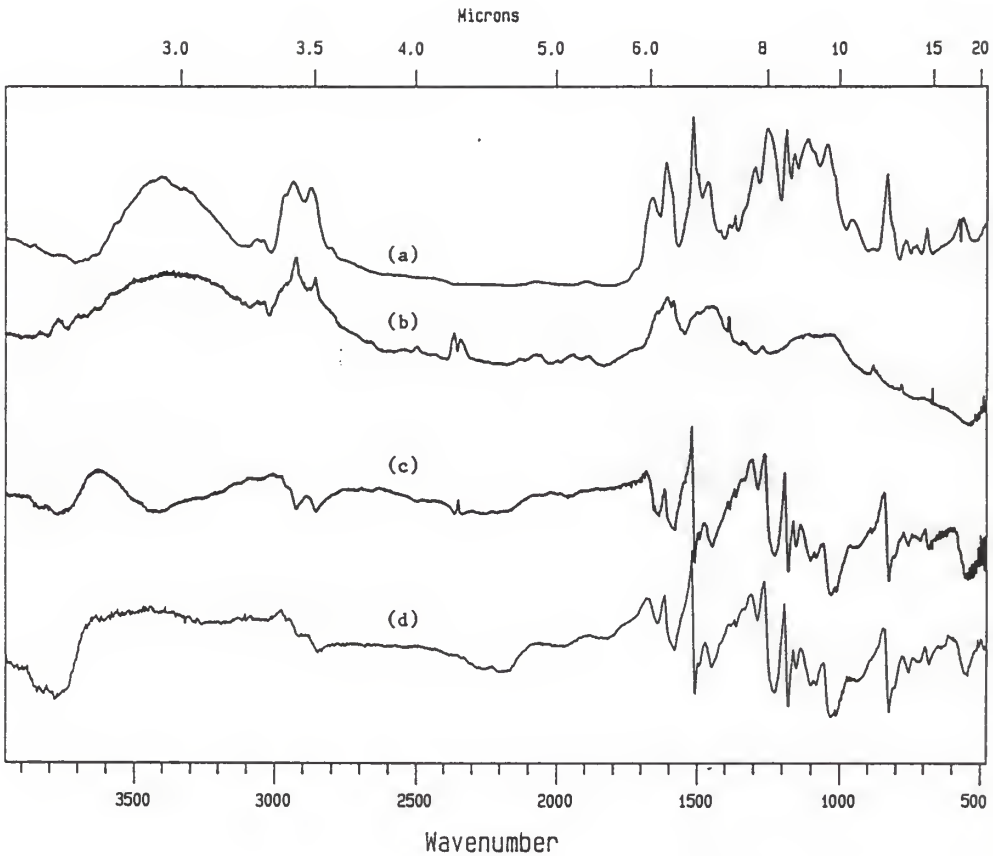


Figure 10: 0 mils KBr overlayer and specular reflection spectra of EC3448 80% humidity prebond exposure cast film sample. (a) Transmission spectra as a reference. (b) 25 mil KBr overlayer as a reference. (c) 0 mil KBr overlayer. (d) Specular reflection spectra.

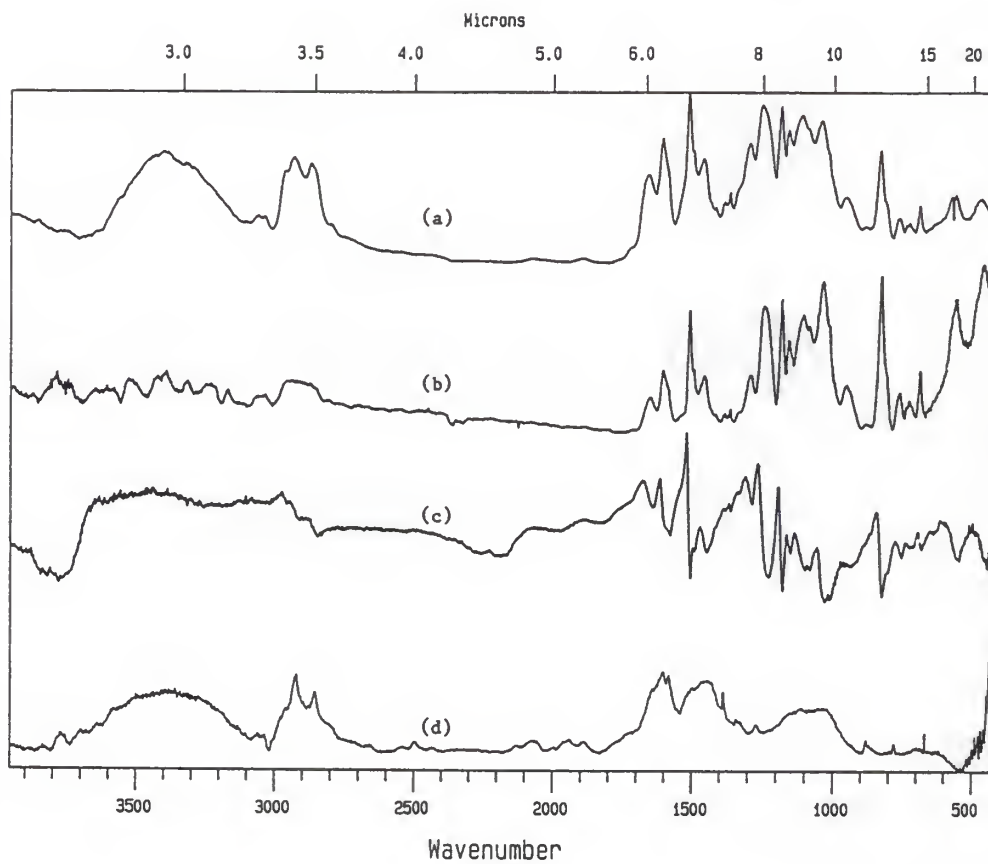


Figure 11: FT-IR spectra of EC3448 80% humidity prebond exposure.  
(a) Transmission. (b) Attenuated Total Reflectance.  
(c) Specular reflection. (d) 25 mil KBr overlayer.

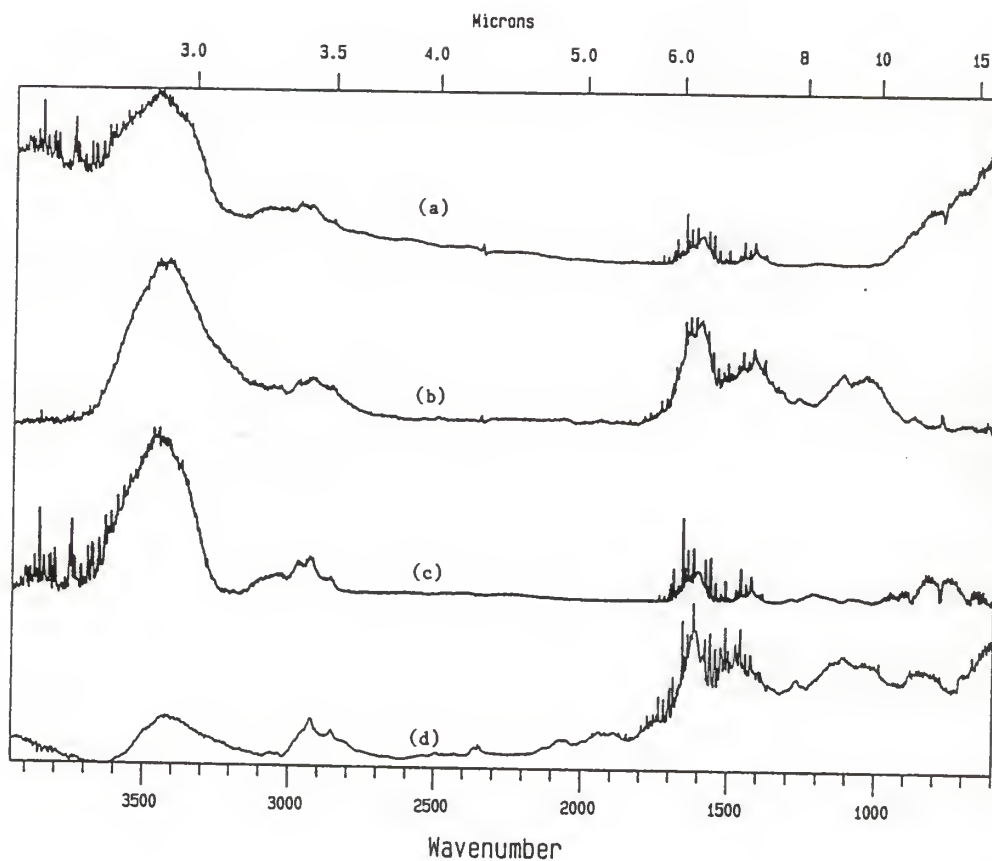


Figure 12: 45 mil KBr overlayer spectra of fractured adhesive samples. (a) A19 80% humidity prebond exposure. (b) EA9304.1 80% humidity prebond exposure cast film adhesive. (c) A72 room humidity prebond exposure. (d) EA9304.1 room humidity prebond exposure cast film adhesive.

### Reference

- (1) Grove, R.A., Volume 1: Engineering Materials Handbook, Composites , p.767, ASM International, Metals Park, Ohio (1987).
- (2) DeIasi, R. and J.B. Whiteside, Advanced Composite Materials - Environmental Effects, ASTM STP 658 , pp. 2-20, J.R. Vinson (Ed.), American Society for Testing and Materials (1978).
- (3) Graham, J.A., W.M. Grim III, and W.G. Fately, FTIR, Applications to Chemical Systems, Volume 4, pp.345-391, John R. Ferraro and Louis J. Basile (Eds.), Academic Press Inc., New York (1985).
- (4) Culler, S.R., M.T. McKenzie, L.J. Fina, H. Ishida, and J.L. Koenig, Fourier Transform Diffuse Reflectance Infrared Study of Polymer Films and Coatings: A Method for Studying Polymer Surfaces, Applied Spectroscopy, 38 (6), 791-795 (1984).
- (5) Optical Spectroscopy: Sampling Techniques Manual , Har-  
rick Scientific Corp. (1987).
- (6) McKenzie M.T. and J.L. Koenig, Further Developements in the Methodology of Surface Analysis by FT-IR: Quantita-  
tive Aspects of Diffuse Reflectance Methods, Applied Spectroscopy, 39 (3), 408-412 (1985).



## CHAPTER III

### PHOTOACOUSTIC SPECTROSCOPY

#### MICROPHONE DETECTION

The photoacoustic effect in solids was first discovered by Alexander Graham Bell in the 1880's. Bell found that when a beam of intensity modulated sunlight was focused onto a selenium cell, an audible signal was detectable by nonelectric means; if the sample was enclosed in a cylinder connected to a hearing tube, the photoacoustic signal was greatly enhanced. Further investigation revealed a more noticeable signal was obtained for porous spongy samples than from solid samples. Bell concluded that the nature of the pressure waves that produce the sonorous effects depend upon the material that was exposed to the beam [1]. After the initial discovery by Bell of the photoacoustic effect, little work was done on developing of this technique until more sensitive microphones could be developed.

In the early 1970's, Rosencwaig resurrected this technique by building the first photoacoustic spectroscopy sampling cell [2,3]. Rosencwaig's cell incorporated a microphone to detect the pressure wave generated by the photoacoustic effect. The first IR studies with the PAS cell were carried out using a tunable laser as the excitation source. This did provide sufficient power for the technique, but limited the spectral range that could be examined. A FTIR spectrometer source beam does not have the

same power as a tunable laser; but, with the multiplexing advantages, it has proven to be a good alternate excitation source. Currently there are commercially available PAS cells specifically designed for use in commercial FTIR spectrometers in the market.

The photoacoustic effect in solids is caused by the periodic heating of the sample by a modulated light source impinging upon the sample. At given frequencies of light the solid adsorbs the radiation which causes a transition between vibrational energy levels within the molecules of the sample. Upon relaxing back to their original energy state, the energy adsorbed is released through non-radiative mechanisms. This heat in turn diffuses through the sample to the interface with the deflection media (Figure 1). The heat causes a periodic heating of the deflection media at the interface. As a consequence, a pressure wave is generated that propagates through the medium and is detected by a microphone. In addition to this thermal effect, the periodic heating of the sample causes stresses to be introduced in the sample. The strain is due to the thermal expansion of the sample. Periodic strains in the sample cause a pressure wave to be generated at the interface with the deflection medium. This effect for most deflection mediums at lower modulation frequencies can be considered negligible [4]. At higher frequencies it can become an important component of the photoacoustic signal.

The greatest advantage of FTIR-PAS is in obtaining usable spectra for solid samples without requiring sample preparation. Transmission FT-IR spectroscopy requires either an optically thin sample or incorporation of the sample into a pellet of an IR transparent medium. Attenuated total reflection (ATR) and specular reflection techniques do allow for usable spectra to be obtained on polymer samples without extensive sample preparation. ATR must have the sample to be in intimate contact with the crystal. This type of contact cannot often be realized with solid samples having a rough surface topography. Since PAS monitors only the adsorbed radiation, the interferogram center burst caused by the emission of blackbody sources is eliminated [5]. Solid samples can be monitored under a variety of environmental conditions with the appropriate PAS cell. In situ data can be obtained as long as the gas in the cell does not adsorb in the region of the spectrum under consideration. Microphone detection PAS suffers from the fact that the gases used cannot be corrosive to the microphone. This limits the use of the PAS cell for in situ studies. Vibration isolation of the cell and instrument is needed to minimize the effects of noise from within the room [6].

In addition to analysis of solid surfaces, PAS has been used for in situ studies of surface reactions. Royce used PAS to the study of oxygen inhibition of the photopolymerization of acrylic materials [7]. FTIR-PAS was used by Royce to monitor the change of the number of C=C bonds as the

partial pressure of the oxygen was varied. In this case the oxygen was the gaseous medium used in the PAS technique. In situ FTIR-PAS coupled with electrochemical methods are being developed to monitor the change in surface concentrations of reactive intermediates critical to corrosion processes [8]. In situ studies allow for the measurement of optical properties of the rough surfaces encountered with corrosion. In addition depth profiling can be accomplished. FTIR-PAS has been proven a viable method for studying of electrode/electrolyte interfaces. In situ data coupled once again with electrochemical measurements were obtained on a copper electrode with an orthophosphoric electrolyte [9]. PAS has been compared to transmission spectroscopy for the study of pyridine chemisorbed onto an alumina and silica alumina catalyst [10]. Alumina absorbs pyridine only on Lewis acid sites while silica/alumina absorbs pyridine on both Lewis and Bronsted acid sites. These two sites can be distinguished using spectroscopic methods.

The application of FTIR-PAS to in situ studies of solids is continuing to grow. PAS is limited by the restrictions of the cell design, and the susceptibility of the cell material and microphone to the environment about the sample.

#### PHOTOTHERMAL BEAM DEFLECTION DETECTION

Recently photothermal beam deflection spectroscopy has

emerged as an alternative detection scheme for monitoring a photoacoustic signal generated in solid. Boccara described this mirage effect and its application for observing the photoacoustic signal [11]. The periodic temperature fluctuation of the deflection medium near the sample surface is monitored by a laser beam grazing the surface of the sample. A temperature gradient is induced by the thermal conduction of energy which is released as excited molecules relax from their excited state caused by the absorption of infrared radiation. The deflection of the probe laser beam is a consequence of the thermal gradient at the sample surface changing the index of refraction of the deflection medium (Figure 2). Corresponding periodic changes of the index of refraction lead to probe beam deflections that are correlated to the modulation frequencies, thus obtaining the interferogram. This interferogram is Fourier transformed into the photothermal beam deflection spectra.

The mirage detection scheme depends upon the refractive and thermal properties of the deflection medium. Care is needed in choosing the deflection medium. In addition to the thermal properties, the deflection medium must not absorb in the spectral region of interest for a particular experiment. Fournier demonstrated that comparable sensitivity exists between the gas microphone and mirage detection schemes [12]. PBD spectra were obtained using a air deflection medium, but exceptional vibration isolation had to be undertaken [13]. A 50:1 signal-to-noise ratio was achieved

for the air deflection media by introducing a reference probe beam [14]. The reference beam transverses the same path parallel to the probe beam. The deflections of the reference beam caused by room vibrations and noise are subtracted from the deflections of the probe beam. The change in index of refraction with temperature ( $dn/dT$ ) for a liquid deflection medium is on the order of two to three times greater in magnitude than that of an air deflection medium [15]. Proper choice of a liquid deflection medium provides an enhancement of the sensitivity of the PBD detection scheme.

Photothermal beam deflection techniques can be used in harsh environments which render the electronics in a PAS cell worthless. PBD spectroscopy expanded into the MIR region of the spectrum allows for a variety of surface reactions to be studied in situ that have previously been inaccessible for MIR analysis. Utilizing this technique for in situ studies of electrochemical reactions, catalytic reactions, and liquid phase epitaxy would permit spectroanalysis of these solid/liquid interfaces [15].

PBDS has mainly been used in the ultraviolet, visible, and near-infrared regions of the spectrum. The experimental apparatus incorporates synchronous modulation and lock-in-detection [16]. Trace gas analysis of ethonal in air was accomplished using a He/Ne laser as the probe beam, a CO laser with chopper as the excitation source, and a lock in detection scheme [17]. The experimental results provided



evidence of the high sensitivity of the PBDS technique. Further applications have included the studies of electrochemical process via the PBDS technique [9]. Once again a monochromatic light source with a chopper was used as the excitation source. The use of the PBDS to monitor charge transfer reactions within the solution simultaneously with electrochemical studies provides species specific information.

In situ studies of titanium corrosion by a hot lubricant have utilized PBDS [18]. In this case an argon-ion laser was the excitation source. The deflections at a given wavelength allowed calculation of the number of corroded sites on the titanium surface. Photocorrosion at the ZnSe-electrolyte interface was studied with a xenon source as the excitation beam [19]. However, PBDS utilizing a monochromatic light source limits the spectral range that can be monitored in a given experiment.

Fourier transform infrared PBDS (FTIR-PBDS) incorporates a conventional FTIR spectrometer as the excitation source. The interferometer, being a rapid-scanning instrument, does not allow for lock-in-detection. The detector circuitry must be capable of handling the entire range of input frequencies since all frequencies are being monitored at the same time [14]. Unlike a dispersive instrument the interferometer allows more energy to reach the sample surface since no gratings are needed. The amount of radiation



reaching the surface is crucial to enhancing the photothermal signal.

The development of FTIR-PBDS has been spearheaded for the most part by Low [11,12,15,18,19,20] and Palmer [13,14,21]. The experimental set-up in both efforts are similar. The IR source beam is turned 90 degrees and focused down on to the sample surface (Figure 3). A He/Ne laser separated via a cube beamsplitter into probe and reference beams transversing parallel paths. The probe beam is brought to a tight waist at the focus of the excitation beam at the sample surface. Linear or quadrant array photodiodes monitor the deflection of both beams. The deflections of the reference beam are subtracted from those of the probe beam. This signal is inputted into an A/D converter which generates the interferogram. It has been shown that using a liquid deflection media as compared to a gas increases the deflection of the probe beam by two to three orders of magnitude [16]. Spectra can be obtained utilizing a gas deflection medium with appropriate vibration isolation [14].

The impact of environmental vibrations aspects of FTIR-PBDS has been investigated [20]. Random room vibrations can be diminished by increasing the number of scans that are co-added. Isolating the probe and reference beam from the room environment alleviates deflections caused by thermal effects, air turbulence, and dust in the air. Since the

deflections generated in a gas medium are small, the detectors need to be sufficiently far away as to allow for enhancement of the deflections. A one meter spacing between the sample and detectors has proven to be adequate [21].

If the sample under consideration is IR-transparent, then the reverse mirage technique can be used [15]. The IR beam passes through an optically transparent sample and is brought to a focus at the solid/liquid interface. The probe beam crazes the solid surface at that focus (Figure 4). This technique allows for surface reactions to be monitored where the deflection medium absorbs in the IR region. Solids of interest would be semiconductor material such as silicon, germanium, and gallium arsenide. The reverse mirage technique would be suitable for characterization of electrogenerated species on these semiconductor surfaces [16].

FIGURE CAPTIONS

1. A schematic diagram of the photoacoustic effect with a microphone detection scheme.
2. A schematic diagram of the photoacoustic effect with a photothermal beam deflection detection scheme.
3. A schematic layout of the photothermal experiment utilized by Low and Palmer.

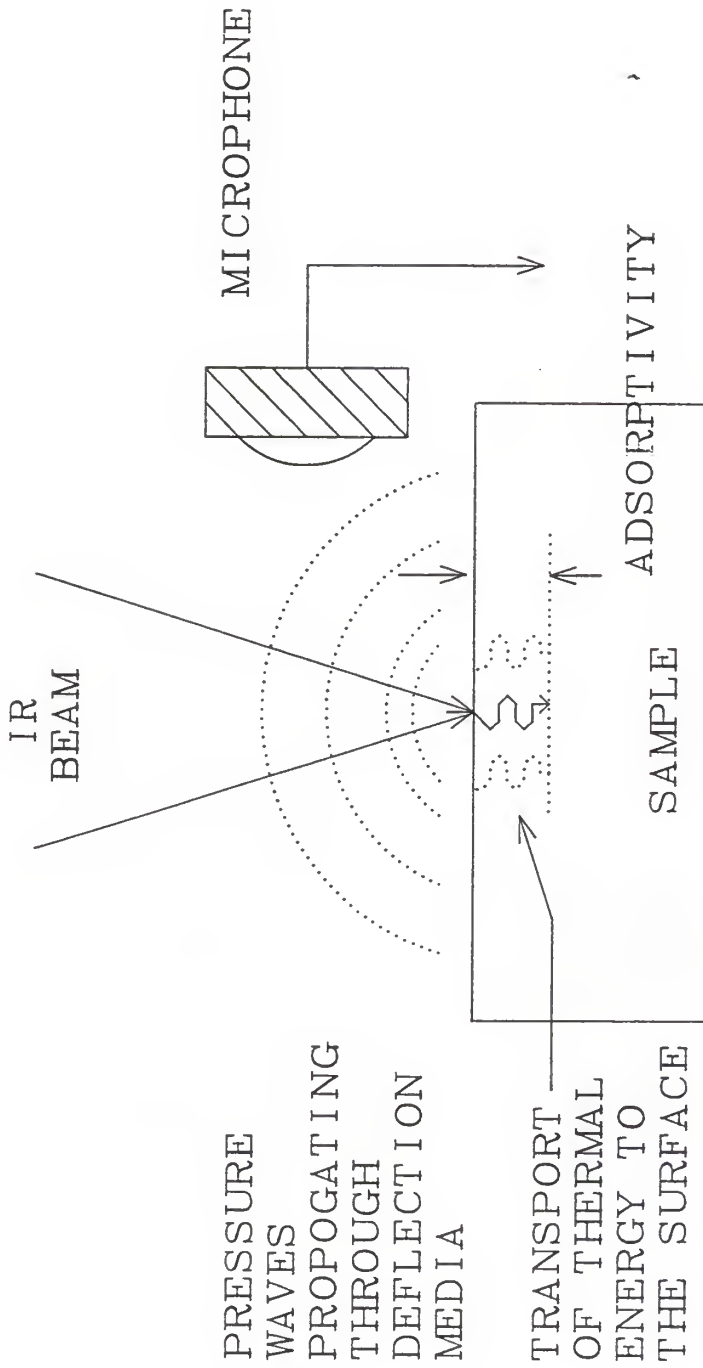


Figure 1: A schematic diagram of the photoacoustic effect with a microphone detection scheme.

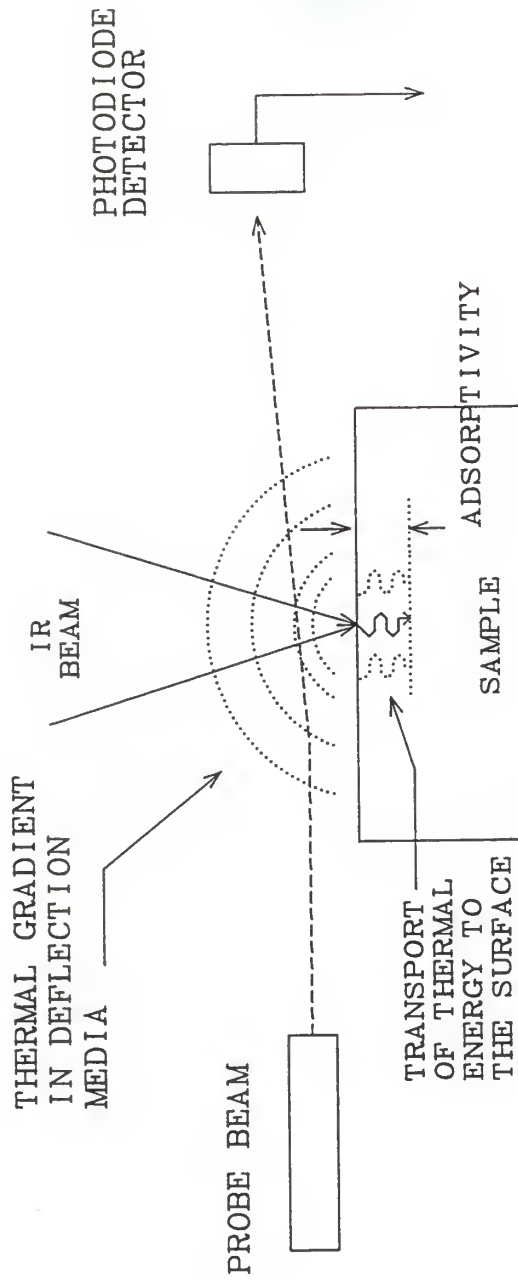


Figure 2: A schematic diagram of the photoacoustic effect with a photothermal beam deflection detection scheme.

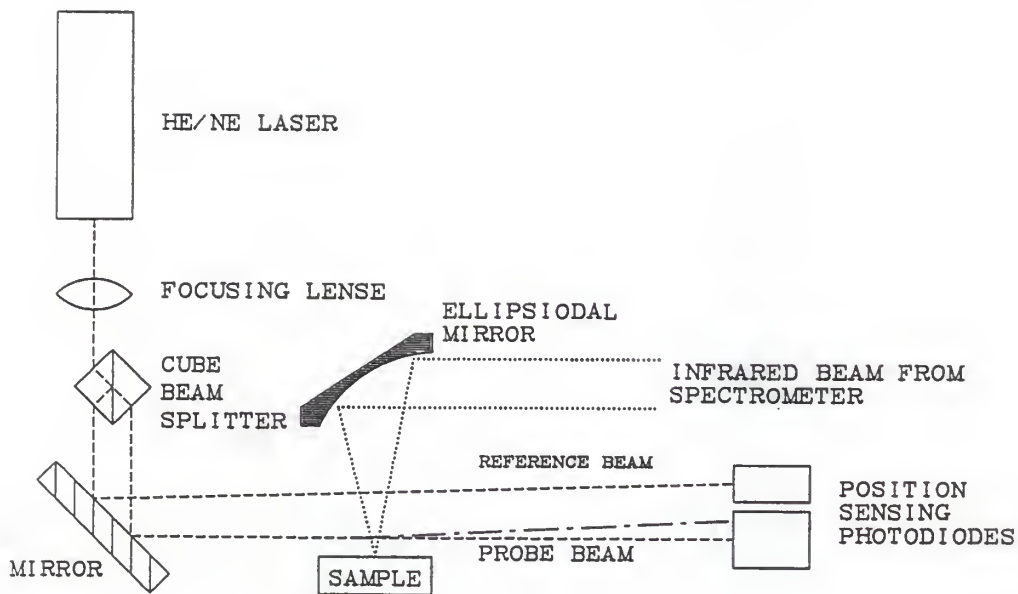


Figure 3: A schematic layout of the photothermal experiment utilized by Low and Palmer.

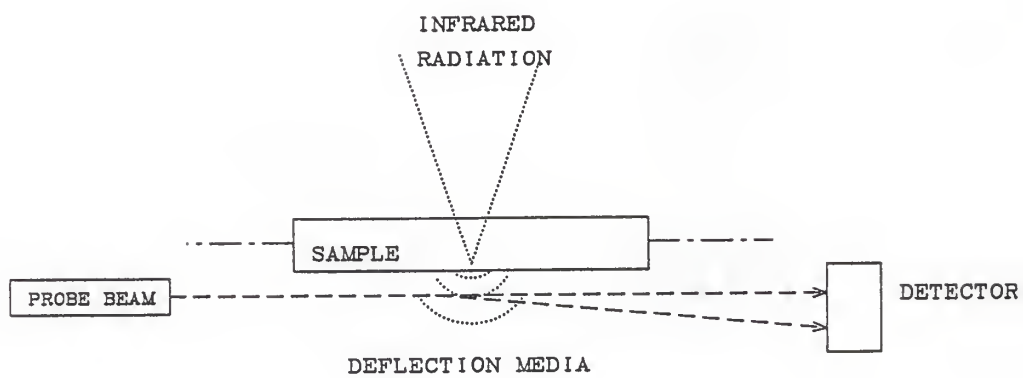


Figure 4: A schematic of the reverse mirage experiment.

### References

- (1) Bell, A.G., American Journal of Science, 20, (1880)
- (2) Rosencwaig, A. and A. Gersho, Theory of the Photoacoustic Effect in Solids, Journal of Applied Physics, 47 (1), 64-69 (1976).
- (3) Rosencwaig, A. and G.C. Wetzal, Theoretical Aspects of Photoacoustic Spectroscopy, Journal of Applied Physics, 49 (4), 2905-2910 (1978).
- (4) Aamodt, L.C. and J.C. Murphy, Thermal Effects in Photothermal Spectroscopy and Photothermal Imaging, Journal of Applied Physics, 54 (2), 581-591 (1983).
- (5) Griffiths P.R. and J.D. Haseth, Fourier Transform Infrared Spectroscopy, pp.9-25, Wiley, New York (1986).
- (6) Royce, B.S.H., A Photoacoustic Study of Chemically Active Systems, Final Report 150983, U.S. Army Research Office, Contract:DAAG29-80-C0053 (1983).
- (7) Royce, B.S.H., D. Voss, and A. Bocarsly, Mirage Effect Studies of Electrochemical Processes, Journal De Physique, 44 (10), 325-329 (1983).
- (8) Vallet, C.E. and G.M. Brown, In Situ Photoacoustic Spectrometry for Corrosion Studies, Oak Ridge National Laboratory, DOE Contract W-7405-ENG-26, CONF-831086--6 (1984).
- (9) Sander, U., H. Strehblow, J.K. Dohrman, In Situ Photoacoustic Spectroscopy of Thin Oxide Layers on Metal Electrodes: Copper in Alkaline Solution, Journal of Physical Chemistry, 85 (4), 447-450 (1981).
- (10) Eyring, E.M., S.M. Riseman, and F.E. Massoth, Catalytic Materials: Relationship Between Structure and Reactivity, pp.399-410, T.E. Whyte, R.A. Dalla Betta, E.G. Derouane, and R.T.K. Baker (Eds.), American Chemical Society, Washington D.C. (1984).
- (11) Boccara, A.C., D. Fournier, and J. Badoz, Contrast Improvement in Photoacoustic and Diffuse Light Fourier Transform Spectroscopy, Applied Physical Letters, 36, 145-150 (1986).
- (12) Jackson, W.B., N.M. Amer, A.C. Boccara, and D. Fournier, Photothermal Deflection Spectroscopy and Detection, Applied Optics, 20 (8), 1333-1344 (1981).



- (13) Low, M.J.D., M. Lacroix, and C. Morterra, Infrared Photothermal Beam Deflection Fourier Transform Spectroscopy of Solids, Applied Spectroscopy, 36 (5), 582-584 (1982).
- (14) Low, M.J.D. and M. Lacroix, An Infrared Photothermal Beam Deflection Fourier Transform Spectrometry, Infrared Physics, 22, 139-147 (1982).
- (15) Smith, M.J. and R.A. Palmer, The Reverse Mirage Effect: Catching the Thermal Wave at the Solid/Liquid Interface, Applied Spectroscopy, 41 (7), 1106-1113 (1987).
- (16) Palmer, R.A. and M.J. Smith, Rapid-scanning Fourier Transform Infrared Spectroscopy with Photothermal Beam-deflection (Mirage effect) Detection at the Solid/Liquid Interface, Canadian Journal of Physics, 64, 1086- 1092 (1986).
- (17) Low, M.J.D., G.A. Parodi, and M. Lacroix, Photoacoustic Cell for Use with Solids, Chem. Biomed. Environ. Instrum., 10 (4), 397-403 (1981).
- (18) Field, R.S., D.E. Leyden, T. Masujima, and E.M. Eyring, Quantitative Applications of Photothermal Beam Deflection Photoacoustic Spectroscopy, Applied Spectroscopy, 39 (5), 753-755 (1986).
- (19) Royce, B.S.H., F. Sanchez-Sinencio, R. Goldstein, and R. Muratore, Studies of Photocorrosion at the ZnSe-Electrolyte Interface by Photothermal Deflection Spectroscopy, Journal of the Electrochemical Society, 129 (10), 2393-2395 (1982).
- (20) Low, M.J.D., Some Practical Aspects of FT-IR/PBDS Part I: Vibrational Noise, Applied Spectroscopy, 40 (7), 1011-1019 (1986).
- (21) Low, M.J.D., C. Morterra, A.G. Severdia, and J.M.D. Tascon, Catalytic Materials: Relationship Between Structure and Reactivity, pp.411-425, T.E. Whyte, Jr., R.A. Dalla Betta, E.G. Derouane, and R.T.K. Baker (Eds.), American Chemical Society (1984).
- (22) Valashkin, P.G. and M.J.D. Low, FT-IR Photothermal Beam Deflection Spectroscopy of Solids Submerged in Liquids, Applied Spectroscopy, 40 (8), 1170-1176 (1986).
- (23) Peoples, M.E., M.J. Smith, and R.A. Palmer, FT-IR Photothermal Beam Deflection Spectroscopy (PBDS) Studies of Polymer-Modified Graphite Electrodes, Applied Spectroscopy, 41 (7), 1257-1259 (1987).

## CHAPTER IV

### FTIR-PAS CELL DESIGN

#### MICROPHONE DETECTION

One of the most important advantages of photoacoustic spectroscopy as compared to conventional techniques is the ability to perform in situ infrared analysis of surface reactions. The type of reactions which can be monitored is limited by the material used to build the sample cells, the amount of infrared adsorption by the deflection media, and the ability of the microphone to withstand the reaction environment. To understand the requirements of cell design for the photothermal beam deflection experiment, a review of the requirements for a gas microphone cell is needed since considerable more data have been obtained with the gas microphone detection scheme as compared to the PBD scheme. Since both detection schemes monitor the photoacoustic effect of condensed phase samples, the requirements for cell design will be similar.

The photoacoustic gas microphone cell consists of two main chambers (Figure 1). In the first chamber there is a sample holder onto which the sample is placed. The sample holder may be a flat post or a sampling cup for powder samples. The sample holder must allow for reproducible alignment of the samples with the focus of the infrared radiation. A window positioned above the sample holder allows

the IR radiation to enter the cell and impinge upon the sample surface. The window must be transparent to the infrared radiation in the spectral region of interest and be resistant to the chemical and thermal environment within the cell. The second chamber contains the microphone. The two chambers are connected via a passage. Gas inlets and outlets are incorporated into the structure of the cell to allow for the deflection media to be introduced. A heating device can be added to allow for studies at higher temperatures.

The first such photoacoustic spectroscopy (PAS) cell was designed by Rosencwaig in 1973. This cell demonstrated that PAS could be used to monitor condensed phase samples in the UV and visible region of the spectra. Since then, numerous types of cells have been built. Currently the most widely used PAS cell is manufactured by MTEC Inc. (Ames, Iowa).

There are many factors that influence the design of a photoacoustic microphone detection cell. The most important factor is to reduce the effect of background signal due to the adsorption of infrared radiation by the walls of the cell. This effect can be subtracted out of the data by ratioing of the sample spectra to a background spectra [1]. A nonabsorbing material, capable of withstanding the cell environment, must be used in constructing the cell which helps reduce the amount of absorption by the cell walls. In

addition, the material chosen as a sample holder must have a low thermal conductivity so as not to interfere with the transport of thermal energy within the sample. The sample holder is positioned in the cell in such a way as to allow for easy loading and unloading of the sample. The most common materials for cell construction are stainless steel and brass. A highly polished wall surface allows for easier cleaning of the cell and reduces the absorption of the infrared radiation by the walls [1].

Unlike cells constructed for the photothermal beam deflection (PBD) scheme, cell design for the microphone detection technique is sensitive to the free volume in the cell. The photoacoustic signal is inversely proportional to the cell volume [1]. The cell normally consists of two chambers. One holds the sample and the other the microphone. These two chambers are connected by a narrow passage. It is desirable to keep the volume of this passage to a minimum. The cell should be nonresonant in the region of the spectra of interest. This will reduce the contribution to noise by the resonance of the cell walls. In order to accomplish this all frequencies generated in the spectral region need to be considered, including the lowest frequencies [1]. One of the most important variables that affects the photoacoustic signal is the distance between the window at which the radiation enters the sample and the surface of the sample. If this distance is less than the thermal diffusion length of the deflection medium, some of the thermal energy

emanating from the sample surface would be absorbed by the window. The thermal diffusion length of the deflection medium is dependant on the modulation frequency. A maximum diffusion length is generated by the lowest modulation frequencies. Thermal diffusion length can be calculated by the following equation.

$$\mu = \left\{ \frac{2\alpha}{\omega} \right\}^{\frac{1}{2}}$$

where

$\alpha$  = thermal diffusivity

$\omega$  = modulation frequency  
and is calculated by:

$$\omega = 2 \nu V$$

$\nu$  = wavenumber of interest [ $\text{cm}^{-1}$ ]

$V$  = Velocity of the moving mirror [ $\text{cm/sec}$ ]

The window must be set at the maximum distance from the sample determined by the thermal diffusion length. Placing the window at a greater distance from the sample would increase the free volume of the cell and thus decrease the photoacoustic signal.

There are two types of microphones, the air condenser and electret-condenser [1]. The air condenser has a response of 50 mV/Pa with a frequency response range of 1 to 5000 Hz. The electret-condenser has a similar response that drops off much quicker at higher frequencies [1].

#### PHOTOTHERMAL BEAM DEFLECTION DETECTION

Cell design for the PBD detection scheme is still in

its early stages of developement. No commercial cell currently exists on the market for PBDS. A PBD cell has the advantage of not requiring the detector to be incorporated within the cell. This allows for in situ studies of reations that are limited with the microphone detection scheme due to the presence of the microphone in the cell.

Palmer has utilized a 1 cm X 1 cm X 1 cm Pyrex cuvette as the sample cell [2]. This cell allows for solid/liquid interfaces to be monitored. The probe laser beam enters and exits on the sides of the cuvette. The cuvette is position on a X-Y-Z movement and tilt precision stage to allow for maximizing of the photothermal signal. The Pyrex cuvette is also used when the reverse mirage effect is being monitored [3]. In this case the IR transparent sample is positioned on top of the cuvette, and the cuvette is filled with the deflection medium to the bottom of the sample.

In Low's initial work on the photothermal beam deflection experiment, ther was no sample cell [4]. The sample was positioned on a post mounted on a precision stage to maximize the signal. A sample cell was designed for Low's later work utilizing an infrared transparent gas as the deflection medium [5]. In this design a quartz UV cell with a KBr window, gas input ports, and a heating coil were incorporated. The extention of Low's work into the solid/liquid interface led to the development of a totally enclosed PBD sample cell in which the environment above the



sample is controlled [6]. The 2.5 cm X 2.5 cm X 1.3 cm. stainless steel cell had a depressed AgCl window on the top to allow the IR radiation to enter the cell (Figure 2). Two holes were pierced into the sidewalls of the cell so that the probe beam could enter and exit the cell. The holes were covered by glass windows to completely isolate the interior of the cell. All cells for FTIR-PBDS described above were developed for sample analysis under mild conditions. No features were added to the cells to allow for high temperature solid/liquid and solid/gas interface in situ analysis.

Masujima, Lloyd, and Eyring's cell design for the study of titanium corrosion by a hot lubricant incorporated many of the features needed for an in situ PBDS cell [7]. The high temperature cell was made out of monel for corrosion resistance. Cell configuration was similar to that of Low's solid/liquid cell. Heat tape wrapped around the monel cell controlled the temperature of the entire cell. Inlet and outlet ports were utilized to regenerate the deflection medium above the sample. The regeneration becomes important when the surface reaction depletes constituents in the deflection medium.

When designing a photothermal beam deflection cell the parameters of the experiment of interest must be considered. The spectral region of analysis needs to be specified. Material selected for the windows and deflection medium will

depend on the spectral region. Windows allowing the beams to enter the cell, as well as, the deflection medium must be transparent in this spectral region. If the deflection medium is not transparent, then modifications of the cell are needed to allow for the reverse mirage experiment. The materials chosen for the windows ,cell walls, sample holder, and seals are influenced by the cell environment. A corrosive environment will require the material chosen to be resistant to the electrolyte. A high temperature cell environment requires the material to be thermally stable in the temperature range, and therefore, having a low coefficient of thermal expansion. Large changes in the index of refraction of the window material leads to misalignment. The materials of all the components in the cell need to be resistant to any aggressive characteristics of the cell environment and be thermally stable in the temperature range of interest.

Once the proper windows and materials have been chosen, the layout of the cell will depend again on the experiment. As stated before the IR window will be placed far enough from the surface as to not interfere with the photoacoustic effect. Appropriate heating devices are added as needed. This will depend on whether it is desired to heat the sample, the deflection medium, or both. Inlet and outlet ports are introduced to allow for regeneration of the deflection medium. Again, this is important if constituents in the deflection medium are consumed or generated.



## CASE STUDY: FTIR-PBDS CELL FOR GALVANIC CORROSION STUDIES

Design of a FTIR-PBDS sample cell for the study of galvanic corrosion will be discussed as a case study. The applicability of FTIR-PBD spectroscopy for surface studies undergoing electrochemical reactions has been investigated [8]. The exposure of metal matrix composites to a saltwater environment leads to a decrease in its mechanical properties [9]. Corrosion in the composite was attributed to the galvanic driving force between the graphite fibers and aluminum. Once the thin skin of aluminum corrodes away by either crevice or pitting corrosion, the graphite fibers and aluminum are exposed to the 3.5% NaCl water solution. For the study of galvanic corrosion with FTIR-PBD spectroscopy the electrolyte would have to be transparent to the IR radiation, if the conventional mirage technique is utilized. The reverse mirage experiment should be used for this case study since the electrolyte is a 3.5% NaCl water solution which is not transparent in the MIR region.

Figure 3 shows a preliminary design of a cell for FTIR PBD in situ studies of galvanic corrosion of an aluminum/graphite system. The cell would be constructed out of stainless steel so as to avoid corrosion of the cell by the electrolyte. A thin layer of aluminum would be deposited on a silicon window. The depth of the layer must be less than the thermal diffusion length of aluminum. A silicon window would be mounted on the cell with the aluminum

facing into the cell. The graphite rod would be inserted into the cell with its surface brought to a few millimeters from the aluminum surface. Two ground glass windows would be positioned on the sides of the cell to allow the focused probe and reference beams to enter and exit the cell. Ports would be added for regeneration of the electrolyte within the cell. The electrolyte would fill the cell completely. A storage tank with a heater would control the temperature of the electrolyte entering the cell. A stage that allows for X-Y-Z and rotational movement would support the cell. Such a stage allows for the photothermal signal to be maximized.

Electrochemical techniques used for predicting galvanic corrosion include potential measurements between the two materials. The graphite and aluminum in the cell would be connected to a zero resistance ammeter. Potentiometric measurements per ASTM:G71-81 would be collected in conjunction with the in situ spectroscopic data. The spectroscopic data would be then analyzed against the electrochemical measurements to correlate the trends observed in both data sets.

FIGURE CAPTIONS

1. A schematic diagram of a simple photoacoustic spectroscopy cell.
2. A schematic diagram of a FTIR-PBD sample cell designed by Low [5] for solid/liquid interface studies.
3. A schematic diagram of a FTIR-PBD sample cell designed for in situ spectroscopic galvanic corrosion studies coupled with electrochemical measurements.

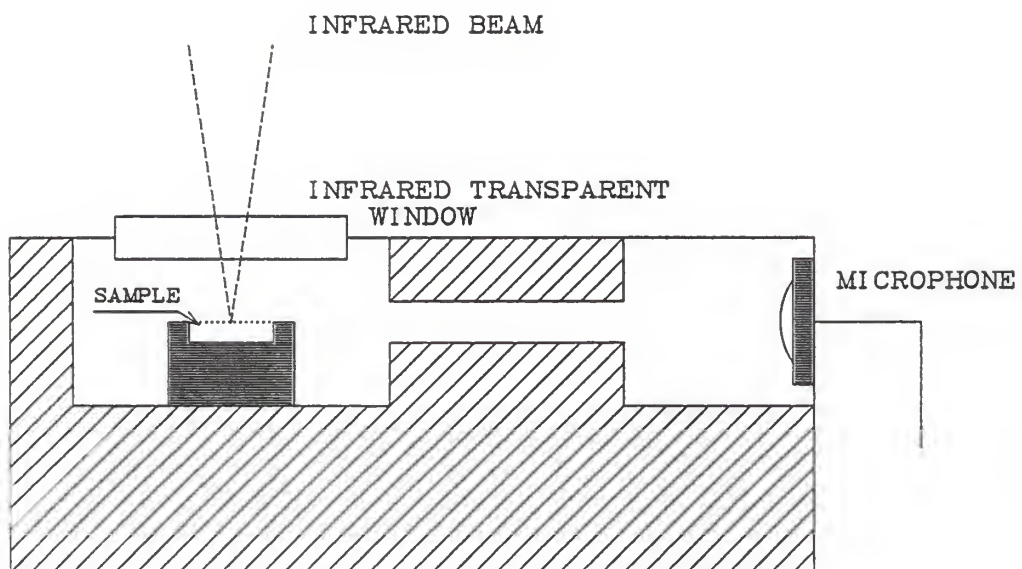


Figure 1: A schematic diagram of a simple photoacoustic spectroscopy cell.

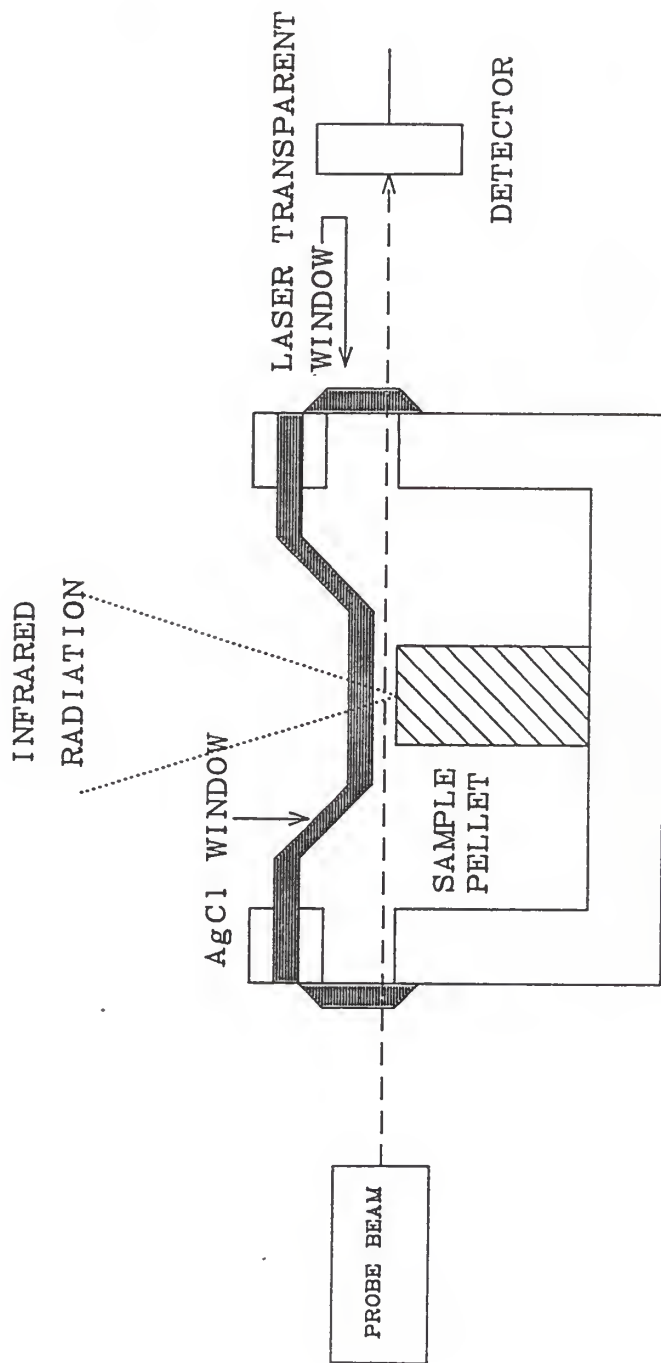


Figure 2: A schematic diagram of a FTIR-PBD sample cell designed by Low [5] for solid/liquid interface studies.

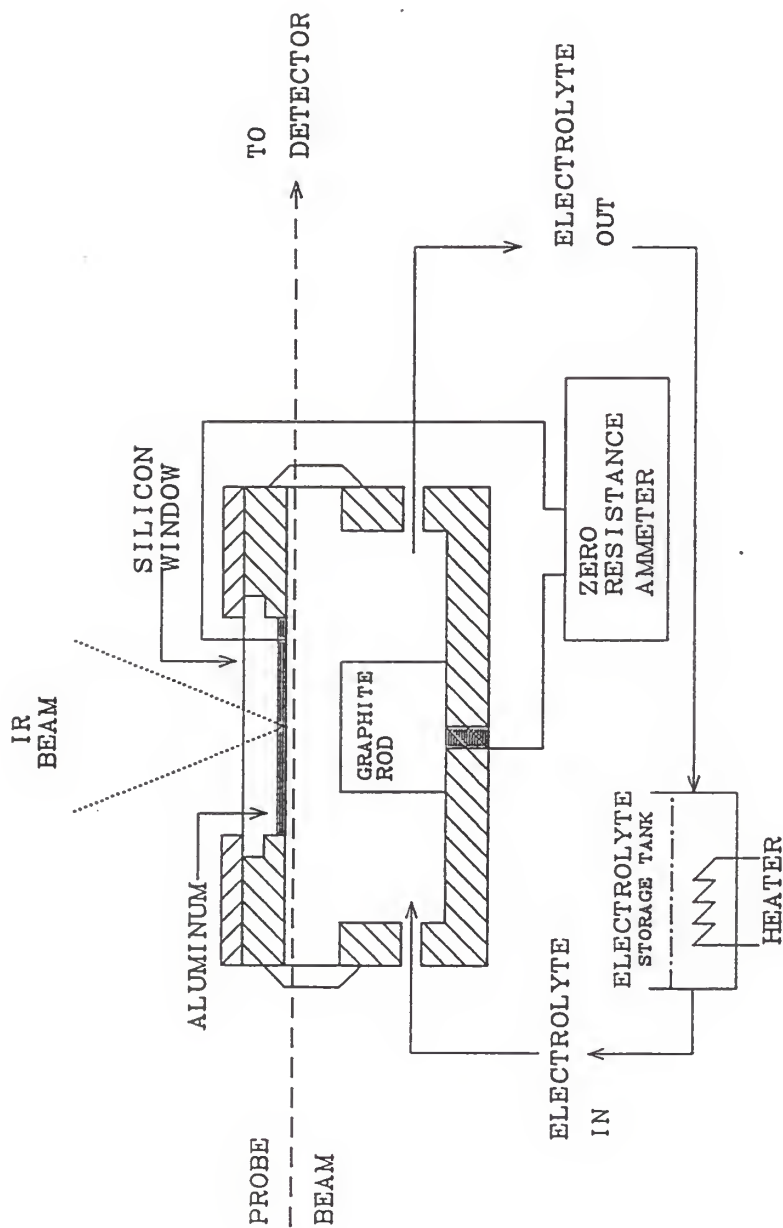


Figure 3: A schematic diagram of a FTIR-PBD sample cell designed for in situ spectroscopic galvanic corrosion studies coupled with electrochemical measurements.

### References

- (1) Graham, J.A., W.M. Grim III, and W.G. Fately, FTIR, Applications to Chemical Systems, Volume 4, pp.341-391, John R. Ferraro and Louis J. Basile (Eds.), Academic Press Inc., New York (1985).
- (2) Palmer, R.A. and M.J. Smith, Rapid-scanning Fourier Transform Infrared Spectroscopy with Photothermal Beam-deflection (Mirage effect) Detection at the Solid/Liquid Interface, Canadian Journal of Physics, 64, 1086-1092 (1986).
- (3) Smith, M.J. and R.A. Palmer, The Reverse Mirage Effect: Catching the Thermal Wave at the Solid/Liquid Interface, Applied Spectroscopy, 41 (7), 1106-1113 (1987).
- (4) Low, M.J.D. and M. Lacroix, An Infrared Photothermal Beam Deflection Fourier Transform Spectrometer, Infrared Physics, 22, 139-147 (1982).
- (5) Low, M.J.D., C. Morterra, A.G. Severdia, and J.M.D. Tascon, Catalytic Materials: Relationship Between Structure and Reactivity, , pp.411-425, T.E. Whyte, Jr., R.A. Dalla Betta, E.G. Derouane, and R.T.K. Baker (Eds.), American Chemical Society, Washington D.C. (1984).
- (6) Valashkin, P.G. and M.J.D. Low, , FT-IR Photothermal Beam Deflection Spectroscopy of Solids Submerged in Liquids, Applied Spectroscopy, 40 (8), 1170-1176 (1986).
- (7) Masujima, T., L.B. Lloyd, and E.M. Eyring, Photothermal Beam Deflection Study of Titanium Metal Corrosion by a Hot Lubricant, Applied Spectroscopy, 38 (6), 804-807 (1984).
- (8) Peoples, M.E., M.J. Smith, and R.A. Palmer, FT-IR Photothermal Beam Deflection Spectroscopy (PBDS) Studies of Polymer-modified Graphite Electrodes, Applied Spectroscopy, 41 (7), 1257-1259 (1987).
- (9) Davis, D.A., M.G. Vassilaros, and J.P. Gudas, Corrosion Fatigue and Stress Corrosion Characteristics of Metal Matrix Composites in Sea Water, Material Performance, 21 (3), 38-42 (1982).

## CHAPTER V

### PHOTOACOUSTIC THEORY

#### BACKGROUND

Theories have been proposed to model the photoacoustic effect in non-gaseous samples since its discovery by Bell in the late nineteenth century. Bell proposed that air expelled from sample pores during periodic heating led to the photoacoustic effect [1]. Lord Rayleigh theorized that thermally induced mechanical vibrations of the sample caused the photoacoustic effect [2]. Toward the close of the nineteenth century Mercadier and Preece added to the list of assumptions that the acoustic wave arises from the periodic heating of the deflection media in contact with the sample [3,4]. All the early theories were never thoroughly examined experimentally.

With the regeneration of interest in the photoacoustic effect in non-gaseous media toward the late 1960's, a more general theory for the photoacoustic effect was developed by Rosencwaig and Gersho [5,6]. The Rosencwaig and Gersho (RG) theory shows that the photoacoustic signal detected by a microphone depends upon the pressure wave generated at the solid/deflection media interface and the transport of that wave to the microphone. The thermal diffusion equations for the solid sample and deflection media are solved simultaneously to generate the temperature gradient in the deflection media. The adiabatic gas law is assumed to calculate the acoustic pressure wave generated by the periodic heating of the sample. McDonald and Wetzel extended Rosencwaig's theory to include the mechanical vibration of the sample surface [7]. Their results show that the acoustic signal is affected not only by thermal coupling but also by acoustic coupling of the



sample. Experimental data have verified the theory developed by Rosencwaig.

Fournier extended Rosencwaig's theory to the photothermal beam deflection detection scheme [8]. Both the transverse and collinear experiments are discussed. Collinear photothermal deflection is where changes in index of refraction are both generated and probed within the sample. The transverse experiment generates and monitors changes in index of refraction in the deflection media adjacent to the sample. The excitation source is a carefully modulated laser beam impinging upon the sample surface. For the transverse experiment the periodic temperature fluctuations in the deflection media adjacent to the sample surface are then related to the probe beam deflection through the temperature dependence of the index of refraction of the media. Aamodt and Murphy further extended Fourniers work by relaxing the assumption that the sample was homogeneous [9].

The derivation of the photoacoustic effect generated within a solid sample and the subsequent deflection of the probe beam which follows, differs from the work of Fournier and Aamodt in that the goal is not an equation for the temperature gradient in the deflection media. This work focuses on developing the equations governing the photothermal signal from a physical point of view. The equations are generated using classical heat transfer theory, after which the derived equations will be put into dimensionless form. Terms in the equations that are most influential in the generation of the photoacoustic signal are easily determined. This will help in properly choosing the parameters to maximize the photothermal signal.

## THEORY

The photoacoustic effect in solids occurs when a modulated light source impinges on the solid surface. Adsorption of particular frequencies results in excitation of the energy levels within the solid. Relaxation from these excited states via non-radiative decay results in energy being released through a thermal process; therefore, a localized, periodic heating occurs in the sample.

This localized heating is transported through the sample and the adjacent deflection media by two mechanisms. The first occurs by conduction. This mode of transport can be modeled using classical heat transfer equations. The second mechanism is known as the thermoelastic process [9]. The thermal elastic process occurs via localized coupling of the thermal energy to the mechanical vibration of the material. This is a non-dissipative process that depends on the speed of sound within the sample and deflection media.

The derivation of the thermoelastic theory follows White's analysis of the thermoelastic effect in condensed phase media [10]. It is assumed that the sample absorbs heat uniformly over the surface defined at a given value of  $x$  (Figure 1). The strain that arises from the temperature fluctuations at the sample surface is given by

$$\epsilon = \frac{\partial u(x,t)}{\partial x} = \alpha_t [T(x,t) - T^*] \quad (1)$$

where

$T^*$  = Ambient temperature of the environment in which the sample is being analyzed

$u(x,t)$  = x-component of surface displacement

$\alpha_t$  = Coefficient of thermal expansion

$T(x, t)$  = Temperature at a given surface,  $x$ , at a specified time  $t$   
The stress-strain relation in the presence of both heating and actual stress becomes:

$$\sigma = B\epsilon - B\alpha_t [T(x, t) - T^\circ] \quad (2)$$

where

$B$  = the bulk modules.

Equation 2 shows that the actual stress is equal to the inherent stress minus the stress caused by the temperature fluxuations. Therefore, if the solid is under compression the inherent stress,  $B\epsilon$ , is negative in sign. A positive change in temperature leads to an increase in compressive stress,  $\sigma$ , while a decrease in temperature leads to a decrease of actual compression. The inverse would hold for inherent tensile stress. A decrease in temperature would enhance the actual stress while an increase would decrease the actual stress.

The equation of motion for an elastic wave traveling in a sample media is given by the following:

$$\rho_s \frac{\partial^2 u}{\partial t^2} = \frac{\partial \sigma}{\partial x} \quad (3)$$

and therefore,

$$\rho_s \frac{\partial^2 u}{\partial t^2} = B \frac{\partial^2 u}{\partial x^2} - B\alpha_t \left( \frac{\partial T}{\partial x} \right) \quad (4)$$

The velocity of sound in a media is defined by the equation.

$$c_o = \left( \frac{B}{\rho_s} \right)^{\frac{1}{2}} \quad (5)$$

Thus, equation 4 can be written as

$$\frac{\partial^2 u}{\partial t^2} = \left( \frac{B}{\rho_s} \right) \frac{\partial^2 u}{\partial x^2} - \left( \frac{B}{\rho_s} \right) \alpha_t \left( \frac{\partial T}{\partial x} \right)$$

$$\alpha_t \left( \frac{\partial T}{\partial x} \right) = \frac{\partial^2 u}{\partial x^2} - \frac{1}{Co^2} \left( \frac{\partial^2 u}{\partial t^2} \right) \quad (6)$$

To solve for  $u(x,t)$ , the temperatures of the solid and deflection media as functions of position,  $x$ , and time need be known. This will now be considered.

It is assumed that the sample is not transparent to the spectral region of interest. For this initial derivation the transport of thermal energy will only occur in the  $x$  direction (Figure 1). The deflection media is assumed to be non-adsorbing in the spectral region of interest. It will be further assumed that all of the energy released in the sample by relaxation processes is converted to heat [9]. These assumptions are valid for most solid samples. In this one-dimensional analysis of the generation of the photothermal signal, the convective mode of heat transfer in the  $x$  direction will be ignored (Figure 1). In addition, heat transfer in the  $y$  and  $z$  direction will be ignored. This assumption can pose problems for some solids, especially those that are inhomogeneous.

Consider the geometry outlined in Figure 1.  $L$  is the thickness of the sample under consideration. The intensity of a sinusoidally modulated monochromatic light source of wavelength  $\lambda$ , at a given position,  $x$ , and time,  $t$ , is given by the following equation [11].

$$I = .5I_0 e^{\beta x} (1 + \cos \omega t) \quad (7)$$

for  $-L \leq x \leq 0$  and  $t \geq 0$

where

$\omega$  = modulation frequency [ $\text{sec}^{-1}$ ]

$I_0$  = incident monochromatic light flux [ $\text{watts/cm}^2$ ]

$\beta$  = optical absorption coefficient of the sample for a given wavelength [ $\text{cm}^{-1}$ ]

The modulation frequency,  $\omega$ , is calculated using the following equation.

$$\omega = 2 \left[ \frac{\text{mirror}}{\text{velocity}} \left( \frac{\text{cm}}{\text{sec}} \right) \right] \left[ \frac{1}{\text{wavelength (cm)}} \right] \quad (8)$$

An energy balance is done for a portion of the sample from  $x$  to  $x+\Delta x$ .  $A$  is the cross sectional area of the infrared beam at the sample surface.

The energy balance for the small slab of sample can be summarized as follows (Figure 2).

$$\left\{ \text{rate of heat} \right\} = \left\{ \text{rate of} \right\} - \left\{ \text{rate of} \right\} + \left\{ \text{rate of} \right\}$$

$$\left\{ \text{accumulated} \right\} = \left\{ \text{heat in} \right\} - \left\{ \text{heat out} \right\} + \left\{ \text{absorption} \right\}$$

$$\Delta x A \rho_s C_s \frac{\partial T}{\partial t} = K_s \left. \frac{\partial T}{\partial x} \right|_x - K_s \left. \frac{\partial T}{\partial x} \right|_{x-\Delta x} A + A \frac{I_0}{2} e^{\beta x} (1 + \cos \omega t) - A \frac{I_0}{2} e^{\beta(x-\Delta x)} (1 + \cos \omega t) \quad (10a)$$

$$\rho_s C_s \frac{\partial T}{\partial t} = K_s \left[ \frac{\left. \frac{\partial T}{\partial x} \right|_x - \left. \frac{\partial T}{\partial x} \right|_{x-\Delta x}}{\Delta x} \right] + \frac{I_0}{2} e^{\beta x} (1 + \cos \omega t) \left[ \frac{1 - e^{-\beta \Delta x}}{\Delta x} \right]$$

A series expansion can be done on the following term.

$$\frac{1 - e^{-\beta \Delta x}}{\Delta x} = \frac{1}{\Delta x} \left[ 1 - \sum_{r=0}^{\infty} \frac{(-\beta \Delta x)^r}{r!} \right]$$

$$\frac{1 - e^{-\beta \Delta x}}{\Delta x} = \frac{1}{\Delta x} \left[ 1 - 1 + \beta \Delta x - \frac{(\beta \Delta x)^2}{2} + \frac{(\beta \Delta x)^3}{6} - \dots \right]$$

$$\frac{1 - e^{-\beta \Delta x}}{\Delta x} = \left[ \beta - \frac{\beta^2 \Delta x}{2} + \frac{\beta^3 \Delta x^2}{6} - \dots \right] \quad (10c)$$

Substituting this result back into equation 10b leads to

$$\rho_s C_s \frac{\partial T}{\partial t} = K_s \left[ \frac{\left. \frac{\partial T}{\partial x} \right|_x - \left. \frac{\partial T}{\partial x} \right|_{x-\Delta x}}{\Delta x} \right]$$

$$\rho_s C_s \frac{\partial T}{\partial t} = K_s \left[ \frac{\left. \frac{\partial T}{\partial x} \right|_x - \left. \frac{\partial T}{\partial x} \right|_{x-\Delta x}}{\Delta x} \right] + \frac{I_0}{2} e^{\beta x} (1 + \cos \omega t) \left[ \beta - \frac{\beta^2 \Delta x}{2} + \frac{\beta^3 \Delta x^2}{6} - \dots \right] \quad (10d)$$

Taking the limit of both sides as  $\Delta x \rightarrow 0$ .

$$\rho_s C_s \frac{\partial T}{\partial t} = K_s \frac{\partial^2 T}{\partial x^2} + \frac{I_0 \beta e^{\beta x}}{2} (1 + \cos \omega t) \quad -l \leq x \leq 0 \quad (10e)$$

where

$\rho_s$  = density of the sample [ $\text{g/cm}^3$ ]

$C_s$  = heat capacity of the sample [ $\frac{\text{cal}}{\text{g}^\circ\text{C}}$ ]

$K_s$  = thermal conductivity [ $\frac{\text{cal}}{\text{cm-sec-}^\circ\text{C}}$ ]

The following initial boundary conditions apply to the solid sample.

$x \rightarrow -l$ ;  $T = T^\circ$ ; the temperature of environment around the sample

$x = 0$ ;  $T = T_s(t)$ ; the surface temperature as a function of time,

$t = 0$ ;  $T = T^\circ$

Equation 10e can be rewritten as

$$\frac{1}{\alpha_s} \frac{\partial T}{\partial t} - \frac{I_0 \beta e^{\beta x}}{2 \rho_s C_s} (1 + \cos \omega t) = \frac{\partial^2 T}{\partial x^2} \quad (11)$$

where

$\alpha_s$  = thermal diffusion coefficient of the solid.

The thermal energy balance in the deflection media is given as follows.

$$\rho_{DM} C_{DM} \frac{\partial T_{DM}}{\partial t} = K_{DM} \frac{\partial^2 T_{DM}}{\partial x^2} \quad (12)$$

$$\frac{1}{\alpha_{dm}} \frac{\partial T_{DM}}{\partial t} = \frac{\partial^2 T_{DM}}{\partial x^2} \quad (12a)$$

Equation 12a is valid if the deflection media doesn't absorb any of the incident infrared radiation. The initial boundary conditions are given as follows.

$$\text{As } x \rightarrow \infty; \quad T_{DM} = T^\circ$$

$$\text{at } x = 0; \quad T_{DM} = T_s(t)$$

$$\text{at } t = 0; \quad T_{DM} = T^\circ$$

Once again the convective mode of heat transfer in the deflection media is neglected. This assumption was valid for the solid sample, but may not always hold for certain choices of deflection media. The temperature gradient generated near the sample surface may lead to free convection heat transfer in the deflection media. These convective currents would cause fluctuations in the probe beam. Taking into account free convection heat transfer the thermal energy equation 12 would be written as follows.

$$\rho_{DM} C_{DM} \left[ \frac{\partial T_{DM}}{\partial t} + v_x \frac{\partial T_{DM}}{\partial x} \right] = K_{DM} \frac{\partial^2 T_{DM}}{\partial x^2} \quad (12b)$$

For this initial analysis the free convection heat transfer mode will be neglected.

The index of refraction of the deflection media in contact with the sample surface is a function of temperature and pressure. The change in the index of refraction which causes the deflection of the probe beam is caused by both an acoustic and thermal effect. The thermal effect is due to the temperature gradient generated in the deflection media causing a change in the index of refraction. The

equations governing this effect for one-dimensional case were derived previously.

The acoustic mode of deflection is caused by two mechanisms. The first is an acoustic wave generated in the sample described by the thermoelastic theory presented earlier. A temperature gradient is developed due to the adiabatic compression of the deflection media [8]. The acoustic wave also causes a deflection in the probe beam by the pressure wave generated at the sample surface. This pressure wave propagates through the path of the probe beam and in turn causes a change in the index of refraction in the deflection media, thus deflecting the probe beam.

The ratio of the acoustic to thermal modes of transport for a gas or liquid deflection media is given as follows [9].

$$\left( \frac{\text{Acoustic Mode}}{\text{Thermal Mode}} \right) \approx 10^{-11} \omega \exp \left( \frac{x_0}{\mu} \right)$$

where

$x_0$  = distance between the sample surface and probe beam

$\mu = \left( \frac{2\alpha_0}{\omega} \right)^{1/2}$  = thermal diffusion length

$\alpha_0$  = thermal diffusivity of the deflection media

$\omega$  = modulation frequency

Consider the mid-infrared region of the spectrum from frequencies of  $4000 \text{ cm}^{-1}$  to  $400 \text{ cm}^{-1}$ . For example, the Cygnus 100 spectrometer's mirror velocity of .02 cm/sec would have corresponding modulation frequencies, calculated using equation 8, of 160 and 16  $\text{sec}^{-1}$  respectively. If, for example, the deflection media is air, it can be



shown that the ratio of the acoustic to thermal mode is indeed small.

Taking  $K_0$  of air to be 0.19 and  $Z_0$  to be the order of 1.0 mm.

$$\left( \frac{\text{Acoustic Mode}}{\text{Thermal Mode}} \right)_{400 \text{ cm}^{-1}} \approx 1.24 \times 10^{-8}$$

$$\left( \frac{\text{Acoustic Mode}}{\text{Thermal Mode}} \right)_{4000 \text{ cm}^{-1}} \approx 3.1 \times 10^{-10}$$

For the mid-infrared region, the contribution to the deflection by the acoustic mode of transport can be ignored. For higher modulation frequencies or larger values of  $Z_0$ , the acoustic mode may need to be included.

Once the acoustic mode of transport of thermal energy is neglected, the change in index of refraction is a function of temperature alone. Consider the following geometry in Figure 3.

The index of refraction can be represented as having a steady-state and fluctuating component.

$$n(x, t) = n_0 + \Delta n(x, t)$$

$$n(x, t) = n_0 + \left( \frac{\partial n}{\partial T} \right)_{T_0} (T(x, t) - T_0) \quad (14)$$

where

$$n_0 = \text{index of refraction at the ambient temperature } T^0$$

The one-dimensional deflection in the x-axis of a laser probe beam can be shown by the following equation [8].

$$\frac{d}{dy} \left( n_0 \frac{dx_0}{dy} \right) = \frac{dn(x, t)}{dx} \quad (15)$$

Substituting equation 14 into 15, an equation relating the deflection  $x_0$  to  $x$ ,  $y$ ,  $t$ , and  $T$  is derived.

$$\frac{d}{dy} \left( n_o \frac{dx_o}{dy} \right) = \left( \frac{\partial n}{\partial T} \right)_{T_o} \left( \frac{\partial T(x, t)}{\partial x} \right)$$

$$\frac{dx_o}{dy} = \frac{1}{n_o} \left( \frac{\partial n}{\partial T} \right)_{T_o} \left( \frac{\partial T(x, t)}{\partial x} \right) y$$

$$x_o = \frac{1}{2n_o} \left( \frac{\partial n}{\partial T} \right)_{T_o} \left( \frac{\partial T(x, t)}{\partial x} \right) y^2 \quad (15b)$$

For small deflection of the probe beam,

$$\tan \phi = \frac{x_o}{y} \approx \phi$$

and therefore,

$$\phi = \frac{1}{2n_o} \left( \frac{\partial n}{\partial T} \right)_{T_o} \left( \frac{\partial T(x, t)}{\partial x} \right) y \quad (16)$$

Equation 16 relates the angle of deflection,  $\phi$ , to  $x$ ,  $y$ ,  $t$ , and  $T$ . For a liquid deflection media  $\left( \frac{\partial n}{\partial T} \right)_{T_o}$  is on the order of two to three times greater in magnitude than that of an air deflection media.  $\phi$ , would be much greater for a liquid deflection media. In order to obtain a similar deflection with a gas media,  $y$  would have to be increased by two or three order of magnitude. This would drastically increase the spatial requirements of the experiment.

Equations 11, 12a, and 15b are put into dimensionless form using the following transformation.

$$\theta = \frac{T(x, t) - T^o}{T^o}$$

$$\chi = \frac{x}{2\pi\mu}$$

where

$$\mu = \left( \frac{2\alpha}{\omega} \right)^{1/2}$$

The thermal diffusion length,  $\mu$ , is a function of the modulation frequency,  $\omega$ . As  $x$  approaches  $2\pi\mu_{DM}$  in the deflection media, the effects of the periodic heating are negligible [9]. Likewise as  $x$  approaches  $-2\pi\mu_s$  in the sample, the thermal effect is essentially damped out. Finally, the dimensionless time,  $\tau$ , is given by

$$\tau = \omega t$$

The initial boundary conditions become

$$\text{at } \chi = 0, \quad \theta = \theta_s(t)$$

$$\chi = -1, \quad \theta = 0$$

$$\chi = 1, \quad \theta = 0$$

$$\tau = 0, \quad \theta = 0$$

Equation 11 can be rewritten in dimensionless form as.

$$\begin{aligned} 8\pi^2 \frac{\partial \theta}{\partial \tau} - \left[ \frac{10\beta(2\pi\mu_s)^2}{2\rho_s C_s} \right] e^{\bar{\beta}\chi(1 + \cos\tau)} &= \frac{\partial^2 \theta}{\partial x^2} \\ 8\pi^2 \frac{\partial \theta}{\partial \tau} - \left[ \frac{2\pi^2 10\beta\mu_s^2}{\rho_s C_s} \right] e^{\bar{\beta}\chi(1 + \cos\tau)} &= \frac{\partial^2 \theta}{\partial x^2} \\ 8\pi^2 \frac{\partial \theta}{\partial \tau} - A e^{\bar{\beta}\chi(1 + \cos\tau)} &= \frac{\partial^2 \theta}{\partial x^2} \end{aligned} \quad (17)$$

$$-1 < \chi < 0$$

where

$$A = \left[ \frac{2\pi^2 10\beta}{\rho_s C_s} \right] \left( \frac{2\alpha}{\omega} \right)$$

$$\bar{\beta} = 2\pi\mu\beta = 2\pi\beta \left( \frac{2\alpha}{\omega} \right)^{1/2}$$

Equation 12a rewritten in dimensionless form is given as follows.

$$8\pi^2 \frac{\partial \theta}{\partial \tau} = \frac{\partial^2 \theta}{\partial x^2} \quad (18)$$

for  $0 \leq x \leq 1$

The deflection of the probe beam equation 15b in dimensionless form is given by

$$\chi = \left[ \frac{\partial v}{\partial \theta} \right]_{\theta=0} \left[ \frac{\partial \theta(\chi_1 \tau)}{\partial \chi} \right] \gamma^2$$

where

$$v = \frac{n}{n_0}$$

$$\chi = \frac{x}{2\pi\mu_{DM}}$$

$$\gamma = \frac{y}{2\pi\mu_{DM}}$$

## DISCUSSION

The dimensionless parameters  $A$  and  $\bar{\beta}$  in equation 17 are both present in the term representing the generation of the thermal energy. These parameters represent the intensity of the thermal energy and the rate at which the energy dissipates as it penetrates into the sample, respectively. Parameters  $A$  and  $\bar{\beta}$  influence both the steady and fluctuating portions of this thermal energy generating term. Both  $A$  and  $\bar{\beta}$  are directly proportional to the thermal diffusivity,  $\alpha$ , and the absorbtivity  $\beta$ , but are inversely proportional to the modulation frequency,  $\omega$ . In addition the dimensionless parameter  $A$  is directly proportional to the energy density,  $I_0$ , and inversely proportional to the sample density,  $\rho_s$ , and heat capacity,  $C$ .

With two parameters  $A$  and  $\bar{\beta}$ , trends in the thermal energy generated can be predicted for various situations. For instance the low modulation frequencies,  $\omega$ , coupled high thermal diffusivities,  $\alpha$ , radiation energy,  $I_0$ , and adsorbtivities,  $\beta$ , would enhance the thermal energy generated within the sample. A less dense sample would increase the dimensionless parameter  $A$ . This fact is true since powder samples will generate a more intense photothermal signal. For the parameter  $\bar{\beta}$ , low modulation frequencies plus high thermal diffusivities and adsorbtivities are desirable. Increasing the value of  $\alpha$  increases the depth of penetration of the infrared radiation into the sample,

therefore, more of the bulk sample would be analyzed.

Dimensionless time  $\tau$ , represents the modulated portion of the thermal energy is dependant on the modulation frequency,  $\omega$ . Large modulation frequencies cause the frequency of the modulated thermal energy to increase. This would be desirable from the fact that the rate of data aquisition increases. High modulation frequencies, as shown previously, decrease the values of  $A$  and  $\bar{\beta}$ , thus decreasing the intensity of the generated thermal energy and the rate of energy dissipation.

To perform a numerical simulation on the following equations, the dimensionless parameters  $A$  and  $\bar{\beta}$  would have to defined. These values would depend on the experiment to be studied. Since numerous data have been obtained on a carbon tetrachloride deflection medium with a carbon black sample, this experiment would be the best choice for initial calculations. The computer algorithm would be written using a finite difference approximation for the equations 17, 18, and 19. The simulation would have to be done for a given modulation frequency. The algorithm would begin at  $X=-1$  using equation 17 and solve up to  $X=0$ . At this point equation 18 would be used up for  $0 \rightarrow 1$ . The program would then check the boundry condition at  $X=1$ . If the boundry condition is met, the program would terminate. Otherwise, it would begin at  $X=-1$  and repeat the process until the boundry condition at  $X=1$  is met. Once the program terminates

the temperature gradient generated by the algorithm would be used along with equation 19 to solve for the deflections. The values obtained from the simulation would then be compared against experimental data obtained for a similar experiment.

Future work would need to concentrate on extending this derivation to the two dimensional case both  $x$  and  $z$ . In addition the effects of the convective eddies on the signal would be incorporated to get a better representation of how the experiment performs. Once the initial algorithm is written and experimentally verified, numerical simulation for various experimental arrangements will provide an insight on the type of signal that will be generated. Thus appropriate modifications can be made to enhance the signal according to the findings from the simulation.

FIGURE CAPTIONS

1. A cross-sectional view of sample with thickness  $L$ . The impinging IR radiation is perpendicular to the surface. The  $X$  coordinate axis is shown.
2. A cross-sectional view of sample with the boundaries  $X$  and  $X - \Delta X$  used for a microscopic energy balance is shown.
3. A schematic of the geometry used in determining the beam deflection.  $X$  is the displacement of the probe beam from the sample surface.  $Y$ , is the distance from the IR focus to the detector.  $X_0$  represents the probe beam deflection.



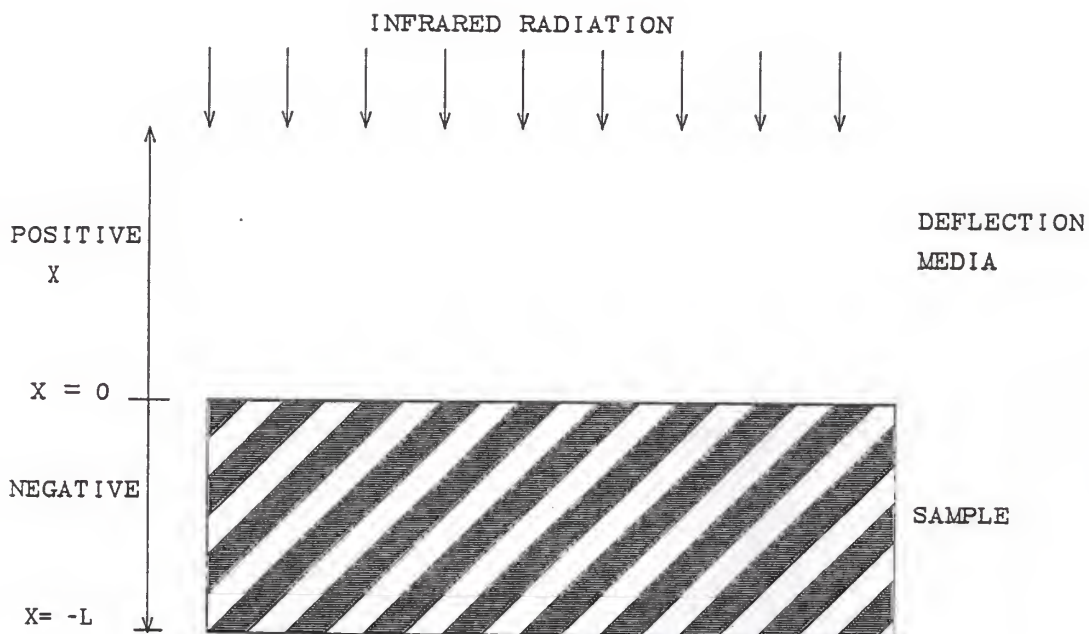


Figure 1: A cross-sectional view of a sample with thickness  $L$ . The impinging IR radiation is perpendicular to the surface. The  $X$  coordinate axis is shown.

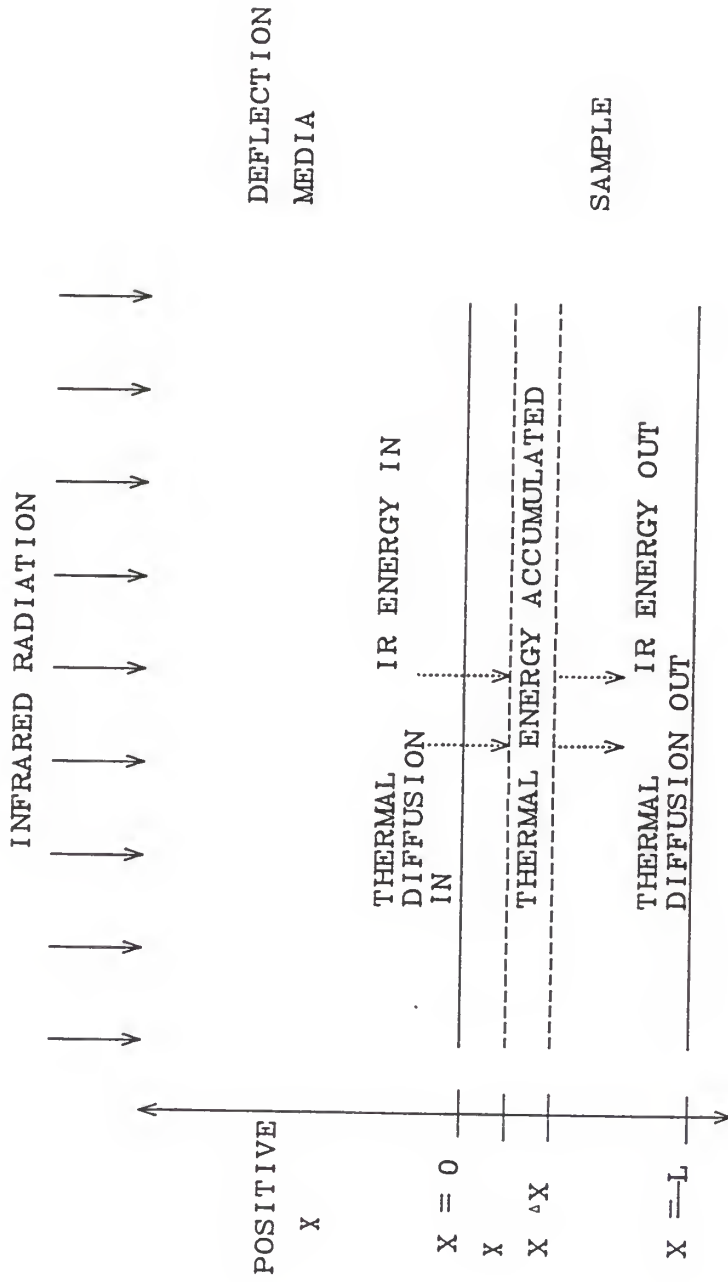


Figure 2: A cross-sectional view of a sample with the boundary conditions at  $X$  and  $X-\Delta X$  used for a microscopic energy balance is shown.

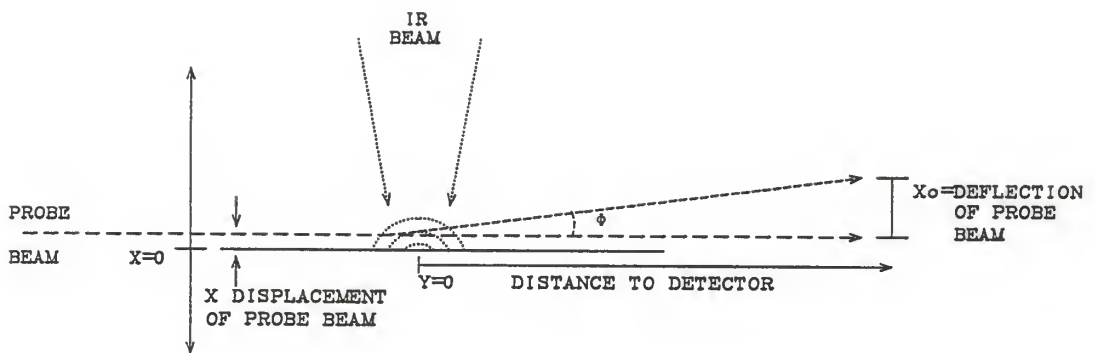


Figure 3: A schematic of the geometry used in determining the beam deflection.  $X$  is the displacement of the probe beam from the sample surface.  $Y$ , is the distance from the IR focus to the detector.  $X_0$  represents the probe beam deflections.

References

- (1) Bell, A.G., American Journal of Science, 20 , (1880).
- (2) Lord Rayleigh, Nature (London), 23 , (1881).
- (3) Mercadier, M.E., Academic Science, 92 , (1881).
- (4) Preece, W.H., Proceedings of the Royal Society of London, 31 , (1881).
- (5) Rosencwaig, A. and A. Gersho, Theory of the Photoacoustic Effect in Solids, Journal of Applied Physics, 47 (1), 64-69 (1976).
- (6) Rosencwaig, A. and G.C. Wetzal, Theoretical Aspects of Photoacoustic Spectroscopy, Journal of Applied Physics, 49 (4), 2905-2910 (1978).
- (7) McDonald, F.A. and G.C. Wetzal, Generalized Theory of the Photoacoustic Effect, Journal of Applied Physics, 20 (8), 2313-2322 (1981).
- (8) Jackson, W.B., N.M. Boccara, and D. Fournier, Photothermal Deflection Spectroscopy and Detection, Optics, 20 (8), 1333-1344 (1981).
- (9) Rosencwaig, A., Photoacoustics and Photoacoustic Spectroscopy, , Wiley, New York (1980).
- (10) White, R.M., Generation of Elastic Waves by Transient Surface Heating, Journal of Applied Physics, 34 (12), 3559-3571 (1963).
- (11) Griffiths, P.R. and J.D. deHaseth, Fourier Transform Spectroscopy, Wiley, New York (1986).

## CHAPTER VI

### INITIAL SET-UP OF FTIR-PBD SPECTROMETER

#### GENERAL SET-UP OF FTIR-PBD EXPERIMENT

All components for the detection of the PBD signal were purchased as separate entities. Care was taken to insure that the parts met or exceeded the requirements given by Palmer [1] and Low [2]. The interferometer used for our photothermal beam deflection experiment is a Cygnus 100 Michelson interferometer. Cygnus is manufactured by Mattson Instruments, Inc. Modifications were made to the unit so that the velocity settings for the moving mirror are decreased by a factor of two, thus the lowest velocity setting is .02 cm/sec compared to .04 cm/sec for an unmodified unit. This allows for the modulation frequencies to be decreased to 160 Hz  $\rightarrow$  16 Hz over the frequency range from 4000  $\text{cm}^{-1}$  to 400  $\text{cm}^{-1}$ . A flat aluminum coated mirror is mounted into the sampling chamber of the unit to deflect the infrared beam through the external sampling port towards the IR focusing mirror of the photothermal experiment.

Initially the spectrometer was mounted on a one inch aluminum plate sitting on four air vibration isolation supports purchased from Oriel Corp. Sampling optics were mounted on a honeycomb air table purchased from Oriel Corp. The table was needed to reduce the effect of building and random room vibrations on the sampling optics. Vibrational isolators on the six inch thick honeycomb table were

effective for room vibrations above 10 Hz. The spectrometer sat on a table separated from the sampling optics table completely (Figure 1). This was done in hopes of reducing the transport of the vibrations from the interferometer to the sampling optics. It was recommended by Dr. William Fately that, in order to have the entire experiment vibrationally coupled, the spectrometer needs to be on the same table as the optics. The instrument was then moved to the air table along with the optics (Figure 2).

The infrared focusing optics consist of a aluminum coated convex mirror mounted to an aluminum frame structure that deflects the infrared beam down to the sample surface. This frame structure holding the IR focusing mirror was designed by Joel Covey at Mattson Instruments. The infrared beam is brought to a tight focus at the focal length of the mirror (Figure 3). A He/Ne laser purchased from Spectra Physics serves as the probe beam. This 0.5 milliwatt laser is linearly polarized and has a beam diameter of 0.49 millimeters. A laser pointer holding the laser is mounted to the optical table. Specifically it positions the laser beam such that it intersects the focus of the infrared beam. A convex lens with a 155 millimeter focal length focuses the laser beam at its intersection with the focus of the infrared beam. The diameter of the laser beam must be less than that of the infrared beam to minimize the anomalies the photoacoustic signal generates at the perimeter of the excitation spot. Following the focusing lens is a cube beam

splitter which separates the laser beam into two beams, a reference and probe . The cube beam splitter is adjusted until the probe beam intersects the focus of the infrared beam while the reference transverses a parallel path approximately 2 cm to the side of the probe beam. Only the probe beam will intersect the infrared beam. Deflections in the reference beam will be subtracted from those of the probe beam in order to compensate for enviromental disturbances.

Three translational stages, a tilt stage, and two angle plates, are connected to form a sample platform that allows for x, y, z, and tilt adjustment of the sample cell (Figure 4). This platform is positioned under the convex mirror within the aluminum frame structure. A 1.4 cm X 1.4 cm X 2.0 cm ground glass cuvette serves as the sample cell when a liquid deflection media is utilized. If air is the deflection media, a sampling cup similar to that employed in DRIFT spectroscopy is used to hold the sample. Both sample cells are mounted to the sample platform when being used. The cell is then positioned by adjusting the platform such that the focus of the infrared beam impinges upon the sample area to be studied and the probe beam grazes the surface of the sample (Figure 4).

Two United Detector Technology position sensing photodiodes are used to monitor the deflections of both the probe and reference beams. The LSC-30D is a continuous single axis position cell that detects linear movement of a light

spot. The photodiodes come with an active surface of 122 mm, and provide a resolution of .0005 inches. Each detector is mounted on a one inch sleeve attached to vibrationally damped rod bolted to the air table. This sleeve allows for the adjustment of the detectors in the z direction. The distance of the detectors to the sample depends on the deflection media being used. In the case of an air deflection media the detectors were positioned one meter from the sample; but, for a liquid deflection media, they are brought to approximately 100mm from the sample since the deflections are on the order of two to three times as great.

The output of the detectors go through a model 301DIV signal conditioning amplifier purchased from United Detector Technology. This transimpedance amplifier conditions the detector signal to provide a position related analog output. The model 301DIV has a frequency range of DC to 5 kHz. Six selectable input ranges can detect signals from 3 microamperes up to 2 milliamperes on the photodiodes. An adjustment pod allows the detectors to be grounded for an output value of 0 volts. A calibration screw on the side of the amplifier is adjusted for a maximum output signal of 10 volts.

The two analog signals from the 301DIV amplifiers are connected to a circuit designed by John Linzi in the Chemistry department at Kansas State University. A schematic of the circuit is shown in Figure 5. A difference amplifier subtracts the reference beam deflections from the probe beam



deflections. This helps minimize effects due to random room and environmental vibrations since the reference beam is subjected to all vibrations the probe beam encounters, except for the photoacoustic effect. Adjustable gain settings of 10X, 100X, and 1000X amplify the subtracted signal. This conditioned analog signal will be put into the spectrometer's A/D converter via an external port. Mattson Instrument's Expert IR software will be used to obtain the data and control the spectrometer.

#### INITIAL ALIGNMENT PROCEDURE FOR THE PBD EXPERIMENT

The alignment procedure described below resembles those presented in the literature [1,2], except for differences due to the lack of similarity in some components. This procedure encompasses the rigorous initial alignment of the experiment utilizing all components described previously. The cube beam splitter which separates the laser beam into a probe and reference beam has been omitted in this initial work. This expedites the alignment of the experiment since numerous adjustments in the set-up are needed initially. Once an initial interferogram has been obtained using the PBD experiment this beamsplitter will be included to provide a reference beam will be added to reduce the random noise in the interferogram due to room vibrations.

The initial tedious alignment of the experiment is required only upon the initial set-up of the experiment.

This procedure will not have to be repeated unless the layout of the experiment is changed or misalignment is suspected. Otherwise, only fine tuning is needed when changing sample cells to maximize the photothermal signal. The procedure is outlined below by referring to Figure 3.

1. Since the infrared beam is difficult to detect via the human eye, a TGS detector or a heat sensitive liquid crystal is used to find the focus of the infrared beam. The TGS detector is mounted on a x, y, and z movement platform and positioned under the focusing mirror. The output of the TGS detector is connected into the A/D converter in the spectrometer via its external port. Observing the center burst signal on the monitor of the Chemist's Workbench using the tune subroutine of the Expert IR software, the TGS detector is adjusted so as to maximize the center burst signal.
2. The laser beam is adjusted with the aid of the laser pointer assembly to intersect the photodiode in the TGS detector at the focus of the impinging infrared beam.
3. A convex lense is then positioned on the optic table to focus the probe beam at its intersection with the infrared focus. This is easily accomplished by adjusting the lense so the back reflection of the laser intersects the beam opening in the laser tube. Care must be taken to insure the probe beam is still intersecting the infrared focus.

4. The cube beam splitter is mounted after the focusing lense to split the laser beam into the reference and probe beam. Adjustments are made so that the reference beam is approximately 2 cm to the side of the probe beam which still intersects the infrared focus.
5. The detectors are positioned on the air table at a distance appropriate to whether a liquid or a gas deflection media is being used. With a gas deflection medium, a distance of one meter from the sample to detector is sufficient to obtain deflections of sufficient magnitude. With a liquid deflection media the photothermal deflections are much greater than those in a gas deflection media, and therefore, the distance from the sample to detectors can be decreased. For this initial experiment the distance was approximately 100 mm. Adjust the height of the detectors so that the both the probe and reference beams are hitting the approximate center of the photodiodes in the detectors.
6. Output signal from the detectors are then connected to the Model 301DIV conditioning amplifiers. The output from the amplifiers is connected to the difference amplifier circuitry.
7. The sample cell is mounted on the platform positioned under the infrared focusing mirror. Three translational stages and two angle brackets are used to assemble the platform. Adjustments are made to the sample cell until

the infrared focus is impinging on the area to be studied and the probe beam is grazing the surface of the sample.

8. The analog signal from the difference amplifier is then connected to a 35 MHz Hitachi oscilloscope. Upon chopping of the infrared beam a steady state DC offset is observed on the oscilloscope. By using the adjustment screws at the top of the IR focusing mirror the steady state DC offset is maximized.
9. Once the steady DC offset is maximized the detectors are then grounded to obtain a zero volt output by adjusting the pods located on the sides of Model 301DIV amplifiers.
10. Finally the analog signal from the difference amplifier circuitry is put into the Cygnus's A/D converter via the external port.

When a new sample cell is mounted onto the platform only steps 7 through 10 are needed. The overall alignment of the experiment will remain intact. If the deflection media is changed from a liquid to a gas or vice versa the position of the detectors will have to be changed and steps 6 through 10 repeated.

DISCUSSION OF THE KANSAS STATE UNIVERSITY FTIR-PBD EXPERIMENT

The experimental set-up described previously closely resembles the configurations given by Palmer and Low [1,2]. Some alternative equipment was utilized in hopes of enhancing the photothermal signal. For instance, the excitation source used is a modified Cygnus 100 Michelson interferometer. The slowest optical velocity available is .04 cm/sec, corresponding to modulation frequencies of 160 Hz at 4000 cm<sup>-1</sup> to 16 Hz at 400 cm<sup>-1</sup>. The modulation frequencies are much lower than those reported by Dr. Palmer using an IBM-9195 Genzel interferometer at an optical velocity of 0.235 cm/sec corresponding modulation frequencies from 940 Hz at 4000 cm<sup>-1</sup> to 94 Hz at 400 cm<sup>-1</sup>. The lower modulation frequencies are desirable to maximize the photothermal signal. To obtain similar frequencies as those presented in the literature, the mirror velocity in the Cynus 100 would need to be set at .12 cm/sec. In addition the Mattson spectrometer has one of the more higher energy sources available. As shown in Chapter V, the higher energy source enhances the photothermal signal.

Instead of using a two-quadrant position sensing diode, a continuous linear position sensing photodiode was used. In Dr. Palmer's work he mentions that the maximum distance from the detector to the sample is limited when using a quadrant detector to monitor the probe beam fluctuations in a liquid deflection media [3]. Since the deflection being measured is greater than the active surface of the quadrant detector. With the larger active surface area available on

the continuous linear position sensing diode, large deflections can be observed without exceeding the area available. Typical responses and sensitivities for both types of diodes are similar. A continuous linear detector provides relatively easy alignment, as pointed out by Low [4].

In Low's work the signal conditioning circuitry was built inhouse [4]. Their circuit is similar to that being reported here. However, in this work two conditioning amplifiers matched to the position sensitive diodes were purchased to generate an analog signal for the laser position. The circuit to subtract the reference beam from the probe beam and to amplify the difference signal were built at Kansas State University by John Linzi. Currently this circuitry is being modified using bandpass filters to provide a filtered signal.

To date the apparatus yields the steady state deflection of the probe beam is observed when the infrared beam is impinging upon the surface. This steady state deflection has been shown by Low [5]. If the IR focusing mirror is moved in either direction the steady state offset disappears. As yet the centerburst has not been detected.

Comparing the apparatus at Kansas State University to Palmer and Low, few differences exist. Recent phone conversations with Dr. Palmer suggests the experimental apparatus is set-up and behaving as expected. Dr. Palmer does mention the fact that finding the centerburst riding on top of the

steady-state deflection is the most difficult part of the initial installation. Once the centerburst is found, then the photothermal signal can be optimized.

The PBD experiment has been attempted using both an air and carbon tetrachloride deflection media. The samples used have been carbon black, an adhesive polymer, and lithium carbonate. A steady state deflection in the probe beam was observed when the infrared beam impinges upon the sample surface. For an air deflection media, with the detectors at a distance of 1 meter from the sample, a 800 mV steady state deflection is observed on the oscilloscope for a carbon black powder sample. This voltage reading corresponds to a deflection of the probe beam of 1.2 mm. Using carbon tetrachloride as the deflection media, with the detectors at a distance 250 mm from the sample, a steady state deflection of 2 to 3 volts was observed. The corresponding deflections are 3 mm and 4.5 mm respectively. Low quotes deflections of .8 mm at a detector distance of 100 mm from the sample using carbon tetrachloride as the deflection media [5]. At a 100 mm detector distance our deflections would correspond to approximately to 1.2 mm. Thus the steady state deflections observed in our experiment are similar to or exceed those presented in the literature. The rise time of the steady state deflection was approximately 5 seconds. Again this exceeds Low's observation of 10 seconds [5].

With the infrared beam impinging on the sample surface



deflections of probe beam up to 50 mV can be observed at frequencies between 5 to 10 Hz. These deflections disappear once the infrared beam is blocked. These are due to the convective eddys induced by the bouyancy forces [5]. Low suggests that these low frequency deflections can may be as much as ten times larger than the centerburst [5]. This may be another reason why the centerburst has been so elusive to date. Proper filtering of the signal prior to A/D conversion would eliminate these low frequency deflections.

The electronic noise in our detectors is less than 1 mV rms. Deflections up to 50 millivolts can be observed when someone is walking in the laboratory or the door is slammed. This noise decreases to approximately 5 mV for pedestrian traffic in the hall way. An experiment was conducted to characterize building vibrations prior to mounting the spectrometer on the optical table. A small cup of liquid mercury was mounted onto the sample platform on the air table. The laser was reflected off the mercury's surface and onto the detector positioned 250 mm away. No one was moving in the lab. Deflections of approximately 5 millivolts at frequencies of 5 to 8 Hz were observed. These deflections increased to 50 millivolts once someone started moving around the lab.

#### FUTURE WORK

Future work on the experiment will focus on reducing



the vibrational noise and optimizing the alignment of the experiment. It has been suggested by Dr. Fateley that building vibrations could be reduced by placing the air table on a marble slab and other material. The mass of the marble will help filter out the low frequency building vibrations. Once the experiment is reassembled building vibrations should be examined once again using the mercury experiment. If it is found that the building vibrations are still a problem, the experiment may have to be moved to a more stable room at ground level, in a basement, or to a building with a more rigid structure.

A BNC cable to provide access to the trigger in the A/D converter of the spectrometer has been installed. This will allow triggering of the oscilloscope to coincide with the data acquisition of the computer. A digital storage oscilloscope is invaluable when looking for the centerburst. The external trigger will be connected to the digital scope to permit viewing the entire scan.

During conversations with Dr. Palmer, he suggested that performance of the electronic circuits can be checked using an acoustic generator with a glass slide on top of a speaker. The laser beam will be adjusted to graze the surface of the glass slide. Deflections at a given frequency will be generated by the acoustic generator causing deflection in the laser at that particular frequency. If the detectors and the associated electronics are responding

correctly, the same frequency of deflections will be observed on the oscilloscope.

At John Linzis suggestion the length of the cable connecting the detector to the Model 301DIV conditioning amplifier was shortened to reduce the electronic noise. Shielding was added around the cable to further reduce the noise.

## CONCLUSIONS

The first step of ordering the components required for the photothermal experiment has been completed. All components ordered are similar to those described in the literature by Palmer and Low. The spectrometer, photodiode detectors, and signal condition circuitry purchased are slightly different than those used by Palmer and Low. These specific components have been chosen to enhance the photothermal signal. The apparatus was assembled and initially aligned.

The experiment was attempted with air and carbon tetrachloride deflection media over carbon black, polymer film, and lithium carbonate samples. A steady-state deflection of the probe beam was observed when the infrard beam impinged upon the sample surface. These deflections exceeded those presented in the literature. In addition to the steady-state deflection, 5 to 10 Hz deflections due to the convective eddys induced by the bouyancy forces were observed, as

expected.

As of yet the centerburst in the interferogram has not been detected. By comparing the data obtained from this experiment with those presented in the literature and by phone conversations with Dr. Palmer, the experimental is performing as expected, except residual noise and alignment problems are preventing the centerburst from being observed. Future work will concentrate on reducing the random environmental vibrations in hope of detecting the centerburst. Other experiments will be conducted to confirm that the response of the detectors is sensitive enough to detect the centerburst.

FIGURE CAPTIONS

1. A schematic diagram of the PBD experiment with the spectrometer located on a separate table. (a) Front view. (b) Side view.
2. A layout of the PBD experiment with the spectrometer mounted on the optical table along with the experiment's optics.
3. A sideview of the probe beams focusing optics mounted on the optical table.
4. A schematic diagram of the sample cell's X, Y, Z, and tilt positioning stand.
5. A diagram of the difference amplifier built by John Linzi at Kansas State University.
6. A plot comparing the steady-state deflection of the probe beam observed at Kansas State University versus that observed by Low. The deflections correspond to a carbon tetrachloride deflection media with a carbon black sample.

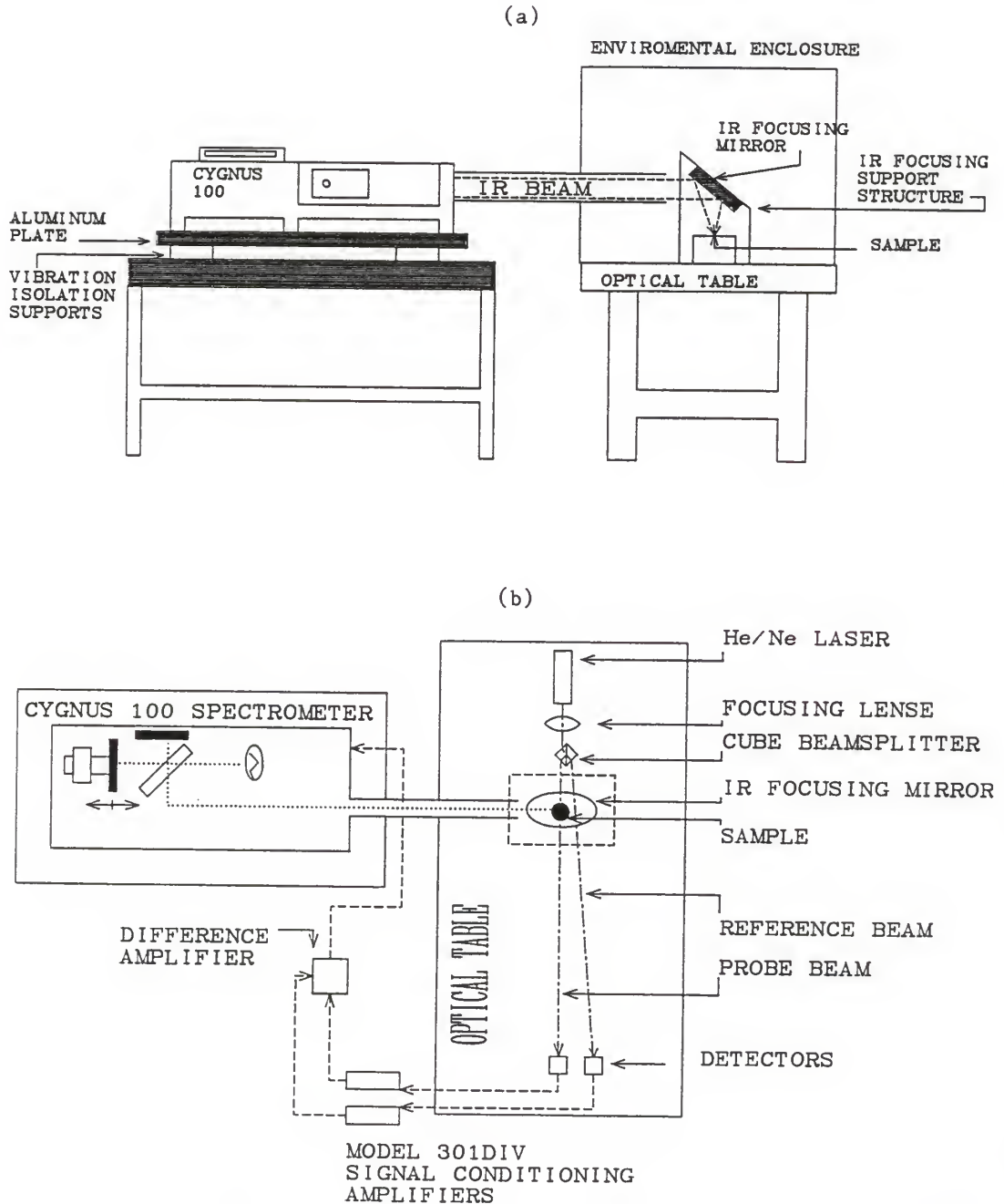


Figure 1: A schematic diagram of the PBD experiment with the spectrometer located on a separate table. (a) Front view. (b) Side view.

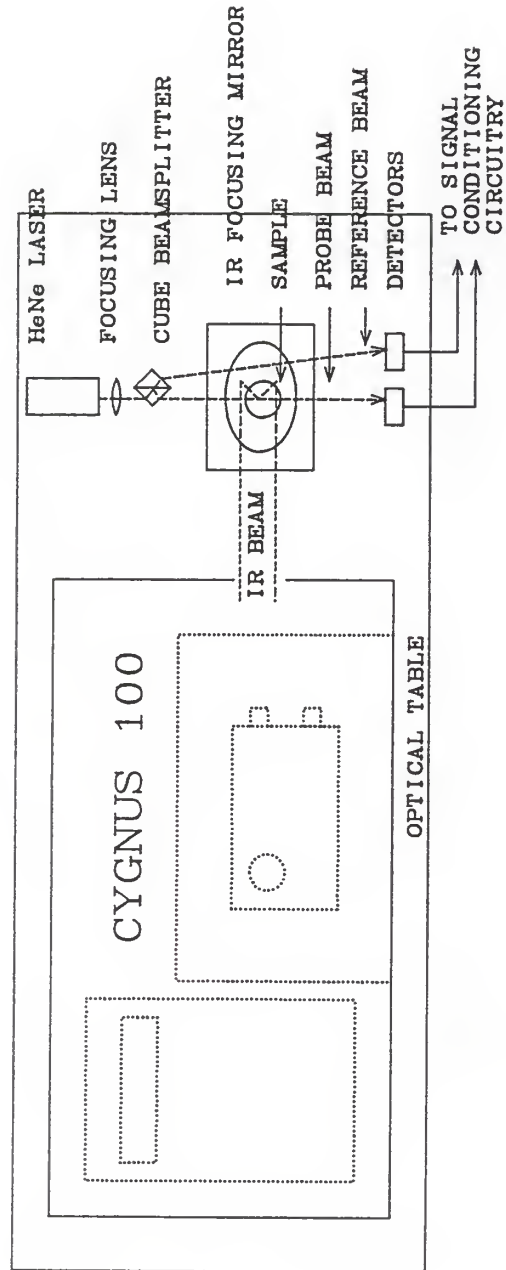


Figure 2: A layout of the PBD experiment with the spectrometer mounted on the optical table along with the experiment's optics.

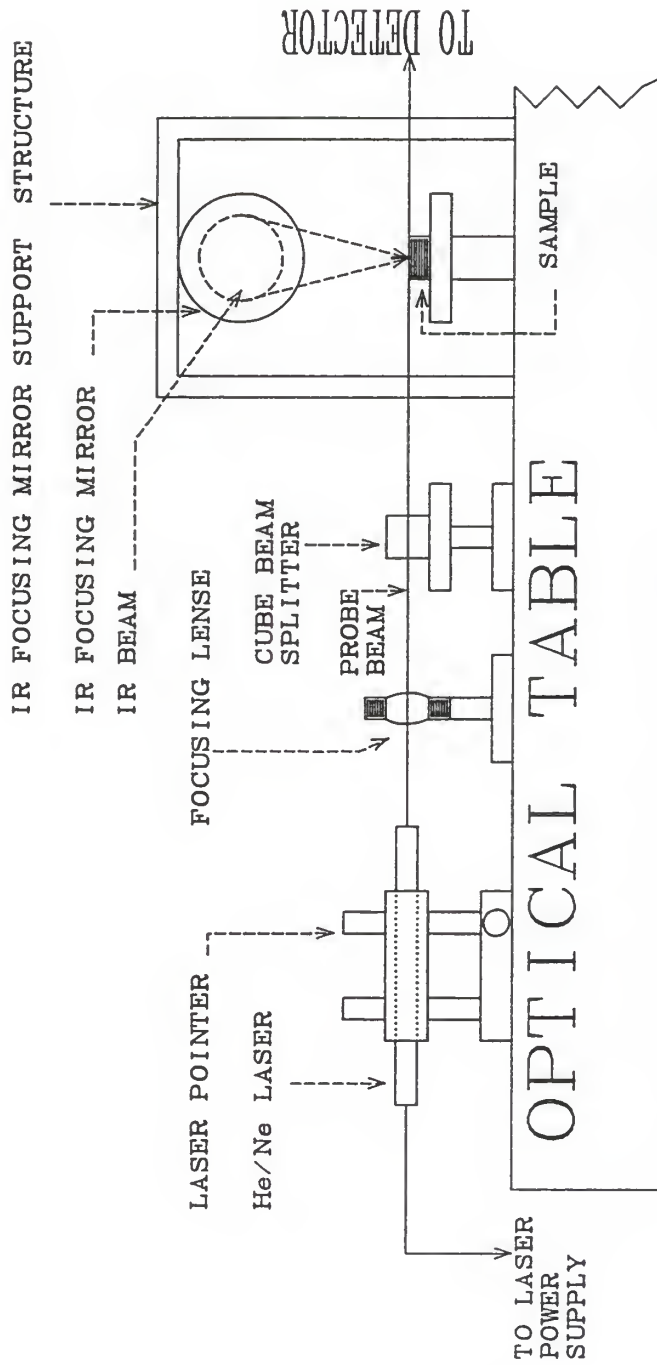


Figure 3: A sideview of the probe beams focusing optics mounted on the optical table.

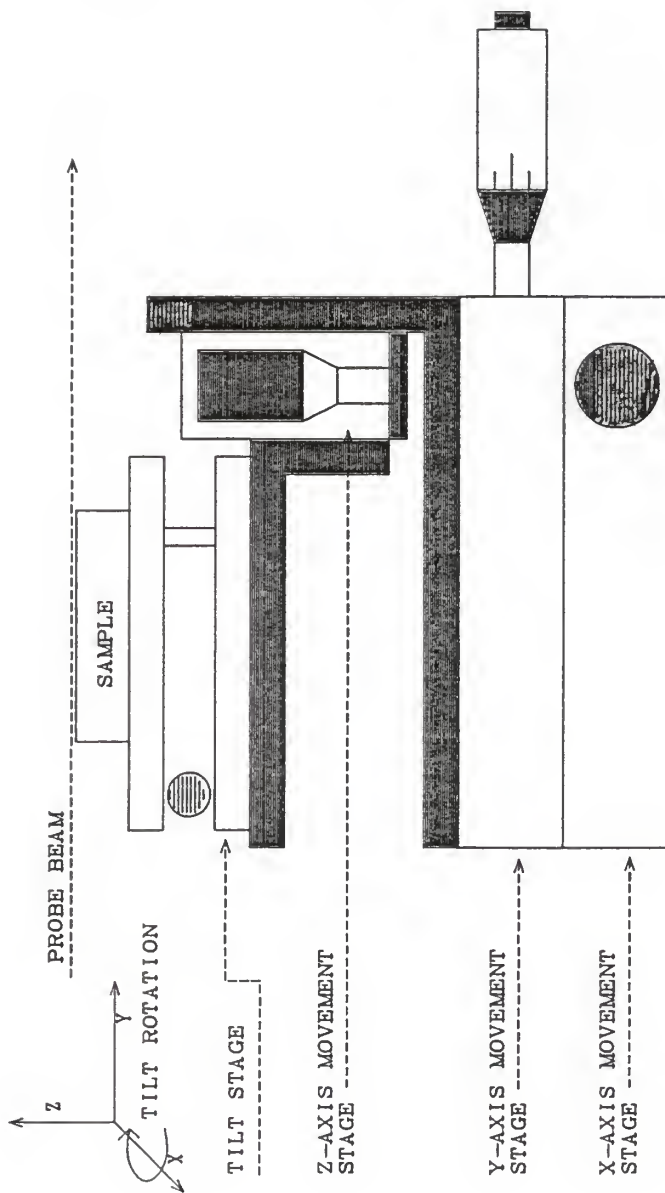


Figure 4: A schematic diagram of the sample cell's X, Y, Z, and tilt positioning stand.



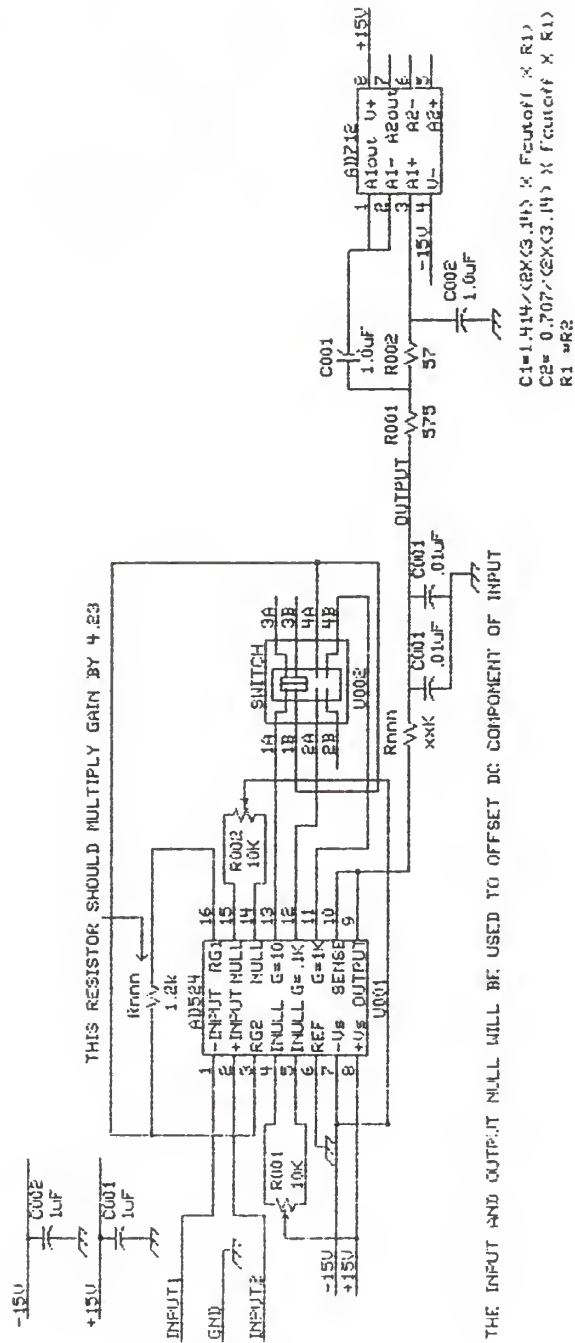


Figure 5: A diagram of the difference amplifier built by John Linzi at Kansas State University.

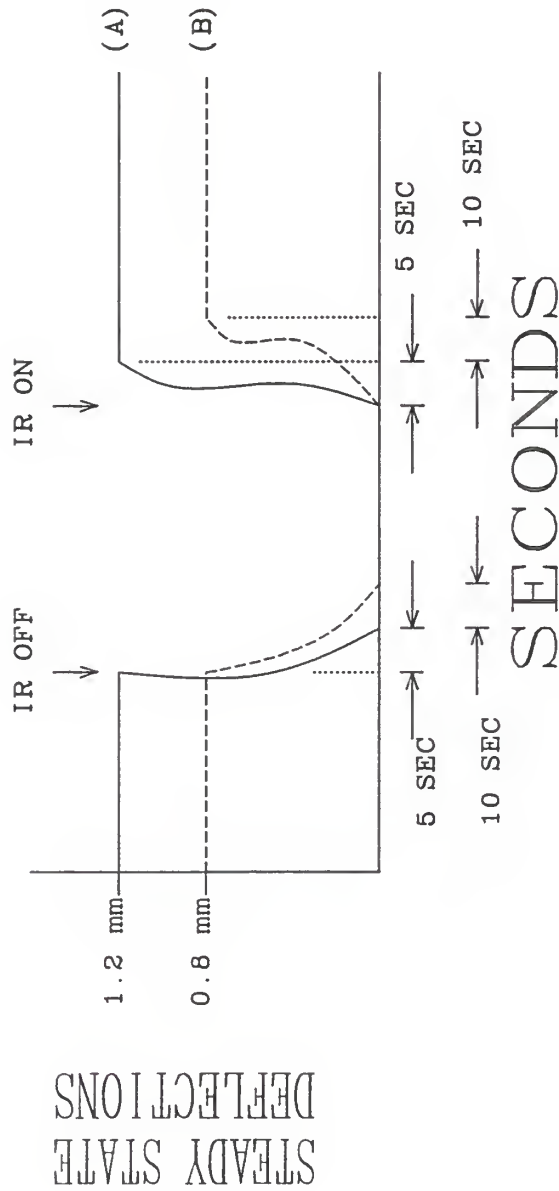


Figure 6: A plot comparing the steady-state deflection of the probe beam observed at Kansas State University versus that observed by Low. The deflections correspond to a carbon tetrachloride deflection media with a carbon black sample.

References

- (1) Smith, M.J. and R.A. Palmer, The Reverse Mirage Effect: Catching the Thermal Wave at the Solid/Liquid Interface, Applied Spectroscopy, 41 (7), 1106-1113 (1987).
- (2) Low, M.J.D. and M. Lacroix, An Infrared Photothermal Beam Deflection Fourier Transform Spectrometry, Infrared Physics, 22 , 139-147 (1982).
- (3) Peoples, M.E., M.J. Smith, and R.A. Palmer, FT-IR Photothermal Beam Deflection Spectroscopy (PBDS) Studies of Polymer-Modified Graphite Electrodes, Applied Spectroscopy, 41 (7), 1257-1259 (1987).
- (4) Low, M.J.D., G.A. Parodi, and M. Lacroix, Photoacoustic Cell for Use with Solids, Chem. Biomed. Environ. Instrum., 10 (4), 397-403 (1981).
- (5) Valashkin, P.G. and M.J.D. Low, FT-IR Photothermal Beam Deflection Spectroscopy of Solids Submerged in Liquids, Applied Spectroscopy, 40 (8), 1170-1176 (1986).

FOURIER TRANSFORM INFRARED SPECTROSCOPIC TECHNIQUES  
FOR ANALYSIS OF ENGINEERING MATERIALS

by

NICHOLAS CONSTANTINE RIGAS

B.S., University of Missouri at Rolla, 1984

AN ABSTRACT OF A THESIS

submitted in partial fulfillment of the

requirements for the degree

MASTER OF SCIENCE

in

CHEMICAL ENGINEERING

KANSAS STATE UNIVERSITY  
Manhattan, Kansas

1988

## ABSTRACT

The use of Fourier Transform Infrared (FT-IR) spectroscopy for in situ analysis in chemical engineering applications has been examined. A review of FT-IR spectroscopy provides the historical background of the technique and its advantages over the dispersive infrared instrument. The conventional sampling techniques transmission, attenuated total reflectance, and specular reflection are analyzed with respect to their applicability for surface analysis of fractured adhesive composites that have undergone accelerated environmental testing. In addition to the conventional methods, an extension of the diffuse reflection technique in which an overlayer of KBr is introduced over the fractured surface is examined as an alternate method.

A review of photoacoustic spectroscopy including both microphone and photothermal beam deflection detection schemes is discussed. The theory of FT-IR photothermal beam deflection spectroscopy is modeled using the classical thermal transport equations. Cell design for photoacoustic spectroscopy is reviewed and a specific application utilizing the photothermal beam deflection detection scheme examined. The experimental set-up of the photothermal beam deflection experiment is outlined. A discussion of the problems encountered with the initial start-up of the experiment and future recommendations is given.